universität wien

MASTERARBEIT / MASTER'S THESIS

Titel der Masterarbeit / Title of the Master's Thesis

„Directing the transport of active particles using magnetic nanoparticles in an applied field“

verfasst von / submitted by

Martin Kaiser, B.Sc

angestrebter akademischer Grad / in partial fulfilment of the requirements for the degree of

Master of Science (M.Sc.)

Wien, 2018 / Vienna, 2018

Studienkennzahl lt. Studienblatt / degree programme code as it appears on the student record sheet:	A 066 876
Studienrichtung lt. Studienblatt / degree programme as it appears on the student record sheet:	Masterstudium Physik
Betreut von / Supervisor:	Dr. Sofia Kantorovich
Mitbetreut von / Co-Supervisor:	Dr. Pedro Sánchez

Abstract (English)

Microscopic active particles, including self-propelled cells and microorganisms, artificial swimming colloids and nanomotors, have gained a lot of attention due to their relevance in such important fields as biology, biomedicine, nanoscience and nanotechnology. One important aspect in systems of microscopic active particles is to reach an effective external control of their motion. Whereas artificial active particles can be designed to allow such an external control, this feature is difficult to realise for self-propelled cells and microorganisms. By means of extensive computer simulations, we explore theoretically the possibility to control the main direction of motion in a dispersion of generic microscopic active particles by adding to the carrier fluid a viscoelastic bath of ferromagnetic nanoparticles that are known to self-assemble in chains under the influence of external magnetic fields, creating an anisotropic environment with a preferred axis defined by the field direction. We study the influence of the field-assembled structures of nanoparticles on the motion of the active particles, characterising the conditions that provide a higher control of the system. We show that an active particle tends to move along the channels built by chains of ferroparticles and that, depending on the size ration between active and magnetic particles, one can tune the transport efficiency (the ratio of diffusion coefficients parallel and perpendicular to the magnetic field direction) by changing the ferroparticle concentration.

Abstract (Deutsch)

Mikroskopische aktive Schwimmer, wie selbst-angetriebene Zellen und Mikroorganismen oder kunstlich erzeugte schwimmende Kolloide und Nanomotoren, erfuhren in den letzten Jahren ein steigendes Interesse durch ihre Relevanz in der Biologie, Biomedizin, Nanowissenschaft und Nanotechnologie. Ein häufiges Ziel bei der Erforschung aktiver Mikropartikel ist es, eine hohe externe Kontrolle dieser Systeme zu erreichen. Kunstlich erzeugte ak- tive Teilchen können so gebaut werden, dass dies leicht möglich ist, jedoch trifft dies nicht auf Zellen und Mikroorganismen zu. Durch Computer-Simulationen legen wir theoretisch die Möglichkeit dar, die Bewegung eines generischen aktiven Schwimmers durch Zugabe viskoelastischer ferromagnetischer Nanoteilchen in die Trägerflüssigkeit, zu beeinflussen. Diese sind dafür bekannt sich unter einem extern angelegten Magnetfeld zu Ketten anzuordnen und somit eine anisotrope Struktur hervorzurufen. Wir untersuchen den Einfluss dieser Struktur auf die Bewegung eines aktiven Schwimmers und zeigen, dass dieser sich entlang der Ketten und somit entlang der Richtung des angelegten Feldes bewegen. Abhängig von der Größe des aktiven Teilchens, kann so der Transport durch Veränderung der ferromagnetischen Teilchendichte optimiert werden.

Contents

1 Introduction **5**

1.1 Properties of self-propelled particles 7

1.2 Passive Brownian motion 9

1.3 Active Brownian motion 10

1.4 Dynamic models 12

1.4.1 Chiral active Brownian motion 13

1.4.2 Run and Tumble 14

1.5 Diffusion 17

1.6 Self-propulsion mechanisms 19

1.7 Dipole interactions 20

1.8 Getting control over active systems 23

2 Methods **24**

2.1 Molecular Dynamics 24

2.1.1 Velocity-Verlet 24

2.1.2 Langevin dynamics 26

2.1.3 Force calculation 28

2.1.4 Verlet lists 29

2.1.5 Cell lists 30

2.1.6 Instability 31

2.1.7 P^3M-Method 32

2.1.8 Reduced units 36

2.2 Delaunay triangulation 36

2.3 Active Brownian in ferromagnetic fluid 38

2.3.1 ESPResSo 38

2.3.2 Vienna Scientific Cluster 39

2.4 Set-up 39

3 Results **43**

3.1 Size ratio 1:5 43

3.2 Size ratio 1:7 50

3.3 Size ratio 1:10 52

3.4 Comparison between different size ratios 54

4 Conclusion and outlook **56**

Appendices **59**

A Appendix **59**

1 Introduction

In recent years, the interest to systems that are out of equilibrium has been steadily growing. Those systems, reffered to as *active matter*, are not only of physical, but also biological nature. Both have been intensively studied theoretically and experimentally in the past years. The term "active" describes the ability of certain particles or units, to convert energy from their environment into motion, hence, kinetic energy. This property allows them to exhibit properties not reachable by matter in equilibrium. Examples of active matter include systems such as Brownian motors [36], macroscopic animals like insects and even swarm of birds [22, 24], or artificially created self-propelled particles[14, 33] with an example seen in figure 1 (a). The study of systems like these arouses a great hope to discover new physics and eventually new ways of creating devices and materials with applications in all fields of science. Another research topic gaining popularity in the past years, is the behaviour of ferromagnetic nanoparticles and their self-assembling property under external fields. They are by now commonly known to cluster in different shapes and structures and can, amongst other applications, be used to obtain control over a liquid system[31] like, for instance, a suspension of ferromagnetic particles in a solvent as seen in figure 1 (b) . Combining those two phenomena, active matter and self-assembly in ferromagnetic fluids, we used extensive computer simulations to reveal and present in this thesis, novel results if an active swimmer finds itself in a bath of magnetic nanoparticles.

Firstly, the goal of this work is to give a general overview over these highly interesting topics, active matter and magnetic nanoparticles. I start with theoretical models for passive and active Brownian motion, covering different dynamic models, such as SET- and RH-model. A summary of run-and-tumble dynamics is also given to show a contrast to active Brownian motion. Further, diffusion coefficient calculation and diffusion properties of active matter in recent research are shortly presented. Dipolar interactions and their impact on the behaviour of magnetic fluids are discussed, including different possible structures formed by the nanoparticles. The methods

used to obtain our results, are explained to give a more detailed insight into how to utilize computer simulations for finding new dynamical properties of soft matter systems.

All of this, should leave the reader with a basic foundation of active matter, the concept of self-propulsion and comprehension for the methods used.

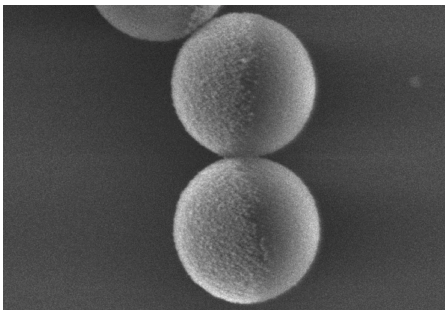

(a) Janus-spheres

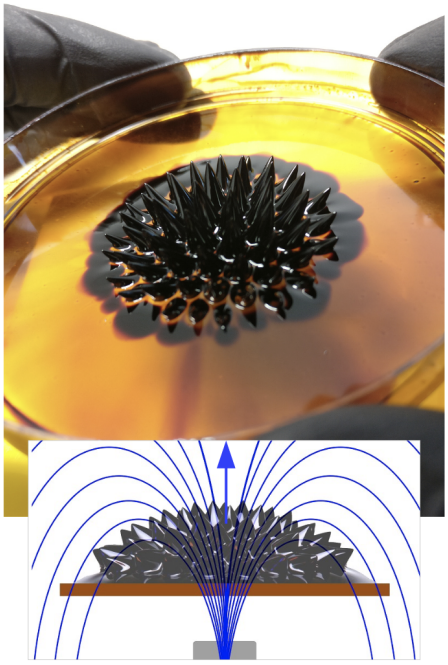

(b) Ferrofluid

Figure 1: *(Close up image of artificially created janus spheres, widely used to study self propulsion (a). The spheres are in the size scale of μm. Picture (b) shows a ferromagnetic fluid under an external magnetic field. The arising spikes form along the magnetic field lines created by the magnet below the petri dish. Picture (b) by Ubaldo M Córdova Figueroa Research Group.*

1.1 Properties of self-propelled particles

Self-propelled particles show major property differences to normal (passive) Brownian particles, as they convert environmental energy to kinetic energy. One of those "out-of-equilibrium-systems" properties, is the interaction rule among particles. If we consider only collisions between self-propelled particles without their environment, momentum is not conserved among them. Additionally, also because we are not in equilibrium, time reversal symmetry is not there anymore.

Another interesting property is the space distribution in the presence of an energy potential and the related cluster formation. With no present forces, particles like gas molecules are uniformly distributed in space and any concentration gradient would lead to a particle flux, which diminishes the gradient itself, restoring homogenous density in the gas. This was introduced in 1855 and is called Fick's law,

$$J = -D\nabla c, \tag{1}$$

where J is the flux, D is the diffusion coefficient and c is the concentration. This behaviour is not always shown in self-propelled particles, because self-propulson alone, without forces between the particles, is sufficient for cluster formation. The cluster formation increases with particle self-propelling velocity and aspect ratio, the ratio of sizes of a geometric shape in different spatial directions [52, 48, 34, 41].

If there are external forces present, Brownian particles are not homogeneously distributed, as they are in a force free case. Macrosocopic quantities, such as particle density ρ, rather follow the Boltzmann distribution,

$$\rho(x) \propto e^{\beta U(x)} \; ; \; \beta = \frac{1}{k_B T}. \tag{2}$$

Here, $U(x)$ is the potential energy, k_B the Boltzmann constant and the total temperature T. Of course, fluctuations of those quantities occur. The density of self-propelled particles does not follow the Boltzmann-distribution[40]. As mentioned above, already without any external potentials, self-propelled

particles tend to cluster and create non-uniform density profiles. The stronger the applied forces are, the bigger the difference to the Boltzmann-distribution gets[40]. I want to quote a simple example for this from *"Dynamics of Self-Propelled Particles: Diffusion, Motility-Sorting, and Rectification"* by Andrea Costanzo[7]: *"Suppose to have a single self-propelled particle confined in one dimension. The particle moves straight and changes its direction of motion at random times. In the presence of a flat potential, the particle distribution will be flat and will therefore satisfy the Boltzmann law. On the other hand, in the presence of potential barriers, which are so steep that the particles can not overcome them, i.e. the external force is stronger than the selfpropulsion force, the density profile will strongly deviate from the Boltzmann distribution. The density profile shows two strong peaks close to the potential walls. This happens since a particle moving in one direction reaches the potential wall and stays there not moving, since the self-propulsion force keeps the particle close to the wall until a random change in the direction of motion happens. The frequency of the reorientation events, i.e. the Peclet number, determines the time for which particles stay close to the walls and therefore the density profile."*

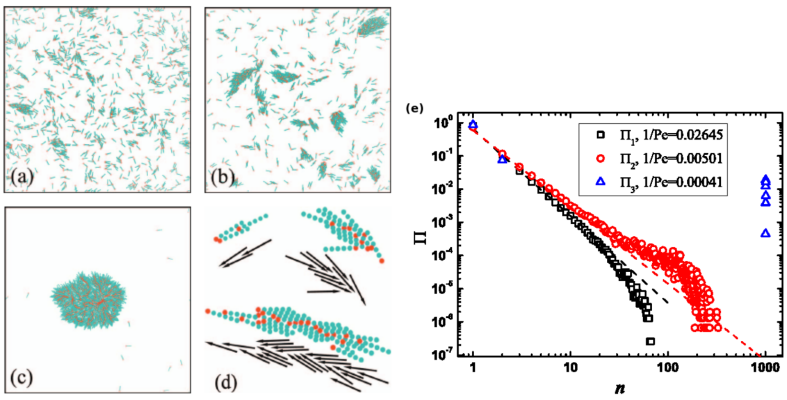

Figure 2: *Simulation snapshots of self-propelled rods froming clusters at increasing Peclet number ((a) lowest, (c) highest), clusters of size n=3,10,22 (d), and cluster size distribution (e). Picture by Yingzi Yang et al., Physical Review E 82.3 (2010)*[51]

1.2 Passive Brownian motion

Before discussing the theoretical description of active particles, it is important to show the differences between active and passive Brownian motion. Passive Brownian particles behaviour is determined by (stochastic) collision of the particle with its surrounding medium. The most common way for the description of such units is Newtonian mechanics considering friction and stochastic forces[26]. The Langevin equation provides the description of motion of a Browinian particle including the Stokes friction coefficient γ in a space dependent potential $U(\mathbf{r})$,

$$m\frac{d\mathbf{v}}{dt} = -\gamma\mathbf{v} - \nabla U(\mathbf{r}) + F(t)\,;\, \mathbf{v} = \frac{d\mathbf{r}}{dt}. \tag{3}$$

With $\nabla U = 0$ in his original publication, Langevin assumed temporally short correlated random forces $F(t)$, independence between coordinate $\mathbf{r}(t)$ and velocity $\mathbf{v}(t)$, and the equipartition theorem $\langle v^2\rangle = 3k_BT/m$. The stochastic forces $F(t)$ should be Gaussian distributed according to Ornstein and Uhlenbeck[42], with independent components and δ-correlated time dependence,

$$\langle F(t)\rangle = 0\,;\, \langle F_i(t)F_j(t')\rangle = 2D_p\delta_{i,j}\delta(t-t')\,;\, i,j = x,y,z. \tag{4}$$

The components of F are called Gaussian white noise with intensity D_p. The noise strength D_p for the momentum, is simply connected with the noise strength for the velocities by the relation $D_p = m^2D$. We can rewrite the Langevin equation as,

$$m\frac{d\mathbf{v}}{dt} = -\gamma\mathbf{v} - \nabla U(\mathbf{r}) + \sqrt{2D}\xi(t), \tag{5}$$

with the stochastic process terms (Gaussian white noise) ξ obeying,

$$\langle \xi(t)\rangle = 0\,;\, \langle \xi_i(t)\xi_j(t')\rangle = \delta(t-t'). \tag{6}$$

We consider now the dynamics in two spatial dimensions. Furthermore we consider a force free, homogeneous environment. A useful representation of the equation of motion is given in polar coordinates, where rotational and translational motions are decoupled. Thus, the equations of motion for a

passive Brownian particle in two dimensions are,

$$\dot{x} = \sqrt{2D_t}\xi_x \,;\, \dot{y} = \sqrt{2D_t}\xi_y \,;\, \dot{\phi} = \sqrt{2D_r}\xi_\phi, \tag{7}$$

where x and y are the coordinates and ϕ the orientation of the particle. $\dot{x}, \dot{y}$ and $\dot{\phi}$ are the time derivates of the quantities, respectively. Since the motion of a passive Brownian particle is purely diffusive, we can give the diffusion coefficient D_t for translational and D_r for rotational diffusion,

$$D_t = \frac{k_B T}{6\pi\eta R} \,;\, D_r = \frac{k_B T}{8\pi\eta R^3}, \tag{8}$$

with T beeing the total temperature and η the fluid viscosity. At this point it is worth pointing out the independence of rotational and translational diffusion coefficient of the particle radius R. While D_t depends linearly on R, D_r depends on the third power of R.

1.3 Active Brownian motion

As shortly mentioned above, active particles can be biological agents and, therefore, for example macroscopic animals, or artifical particles. If investigated, it is most likely to find that they have a preferred direction of motion. This can occur due to asymmetries of the swimming body, which is more obvious for organic organisms, but also because of differences in the propulsion mechanism[19, 29]. There are also several examples of synthetic self-propelled particles at different length scales with a prefered orientation. These include chemically powered particles, like the so-called Janus particles, coated on one side with one material and on the other side with another material, such that the chemical reactions of the materials with the environment produce a net constant force on the particle which is then self-propelled[45, 50]. This orientation is called *heading* and is defined now without any further knowledge about the origin. The heading is then simply defined by a time dependent unit vector $\mathbf{e}_h$, which is, if we again consider two dimensions as above, determined by a single angle ϕ,

$$\mathbf{e}_h(t) = (cos(\phi(t)), sin(\phi(t))). \tag{9}$$

The velocity v can be either positive or negative and is then called going forwards or backwards with respect to the heading. We can write the velocity vector as $\mathbf{v} = v\mathbf{e}_h$, using the heading unit vector introduced above. To span all of the two dimensional space, a second vector is needed. For this we can take the angular direction perpendicular to the heading direction,

$$\mathbf{e}_\phi(t) = (-sin(\phi(t)), cos(\phi(t))). \tag{10}$$

Figure 2 schematically shows the idea with heading and velocity of a polar particle in motion.

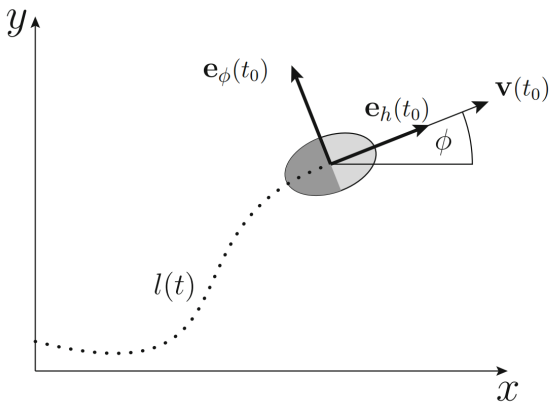

Figure 3: *Visualization of a moving polar particle with heading unit vector $\boldsymbol{e}_h$ and angular unit vector $\boldsymbol{e}_\phi$. The dotted line and $l(t)$ indicates the trajectory. Picture from Romanczuk, Pawel, et al., 2012.[37]*

I wanted to highlight the idea with the heading, to show a simple but important difference between active and passive Brownian particles. While passive "Brownians" don't show a prefered direction of motion, it is often detected on active ones. Below I show how this phenomenon manifests itself, leading to the differences in the equations of motion for an active and a passive Brownian. The equations for the passive motion are already written down in equation (7). The equations of motion for an active Brownian particle in two dimensions are,

$$\dot{x} = vcos(\phi) + \sqrt{2D_t}\xi_x \,;\, \dot{y} = vsin(\phi) + \sqrt{2D_t}\xi_y \,;\, \dot{\phi} = \sqrt{2D_r}\xi_\phi. \tag{11}$$

All varibales are the same as in equation (7), ecxept for an additional particle velocity v. We see in contranst, that the new equations are coupled. The reason for that is, that for a self propelled particle the direction of motion is itself subjected to the rotational diffusion[3].

1.4 Dynamic models

We now have equations of motion for an active Brownian particle considering that it has a direction of motion. I would also like to provide a more general approach to the dynamics of active particles, by writing down their Langevin equation as I did before for passive Brownians, see (5). We see there, that we have a constant friction term γ. To realize a particle that self-propells, we consider the friction to be dependent on the velocity.

$$m\dot{\mathbf{v}} = -\gamma(\mathbf{v})\mathbf{v} - \nabla U(\mathbf{r}) + \sqrt{2D}\xi(t). \tag{12}$$

All variables are similar as that in the Langevin equation 5 above and the white noise terms obey to the same rules. Furthermore, mostly a friction coefficient is used that depends non linearly on the velocity, that is negative for small velocities and positive for large ones, also meaning that its zero at some finite speed. The property that the friction can get negative, makes the whole system an "out-of-equilibrium-one".

There are two widely used models for active Brownian particles. One was introduced by Schweitzer, Ebeling, and Tilch[38] and is called the *simplified-depot-model* or *SET-Model*. It uses the friction function

$$\gamma_{SET}(v) = \gamma_0\Big[1 - \frac{\beta}{1+v^2}\Big], \tag{13}$$

which gives rise to self-propulsion for $\beta > 1$. It has zeros at $v = \pm\sqrt{\beta - 1}$, is negative at velocities between and positive beyond these values. Another choice for the friction function is given by Rayleigh-Helmholtz in the *RH-Model*[35, 13].

$$\gamma_{RH}(v) = \gamma_0[v^2 - \alpha], \tag{14}$$

α beeing bigger than 0. The function has zeros at $\pm\sqrt{\alpha}$, is negative between and positive beyond these values.

At this point it is worth pointing out, that in the original model of SET and RH, there is no force term ∇U in the Langevin equation (12). They only use the symmetric friction function. It is though, for several reasons, interesting to consider a non symmetric function. First of all, no symmetric case is generic. As mentioned in section 1.3, active particles may have a preferred direction of motion, such as molecular motors having it along filaments. Also, cells are not always rotationally symmetric which may lead in conjunction with their internal force-generating mechanisms to a drift towards a specific direction. Furthermore, active particles are not isolated in an empty space, but interact with their invironment. Therefore it is interesting to introduce a force term which breaks the symmetry of the system and may lead to the revelation of new dynamical properties.

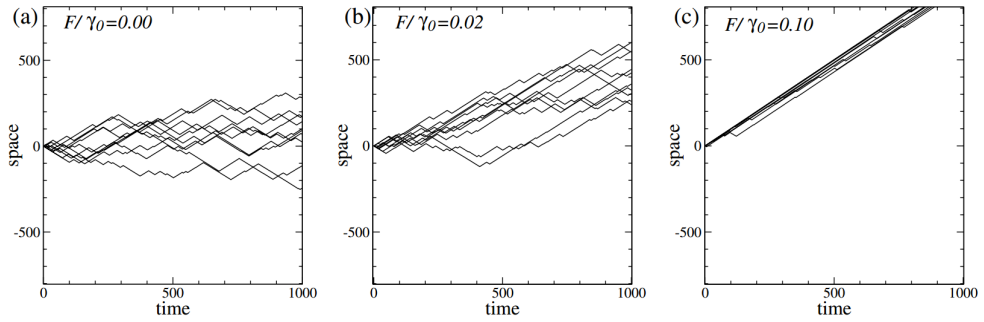

Figure 4: *Trajectories of the RH model obtained by integrating the Langevin equation* (12)*, with noise* $D = 1$ *and* F/γ_0 *0.00 (a), 0.01 (b) and 0.10 (c). There are 10 trajectories in each graph, starting at the same point with parameters* $\gamma_0 = 20$ *and* $\alpha = 1$*. Picture from Romanczuk, Pawel, et al., 2012.[37]*

1.4.1 Chiral active Brownian motion

To have a perfect symmetry along the initial propulsion velocity is an exception and not often to be found on particles. It can be achieved by creating perfect Janus-spheres or rods, but in biological systems the sysmmetry is almost always broken. This leads away from a straight motion to a circu-

lar motion. Even small deviation from the symmetry can make the motion chiral and it is said to be *dextrogyre* if the particle moves clockwise and *levogyre* if it moves counterclockwise. Jennings[18] discovered this behaviour of circular swimming by microoganisms already a century ago and also helical swimming in three dimensions was observed by bacteria and sperm cells[4]. In the following figure, some examples of chiral motion can be seen. In figures 5 (a) and (b), the trajectories of E. coli bacteria near a glass surface and at a liquid-air interface are shown. Figures 5 (c) and (d) show trajectories of artificial L-shaped active particles.

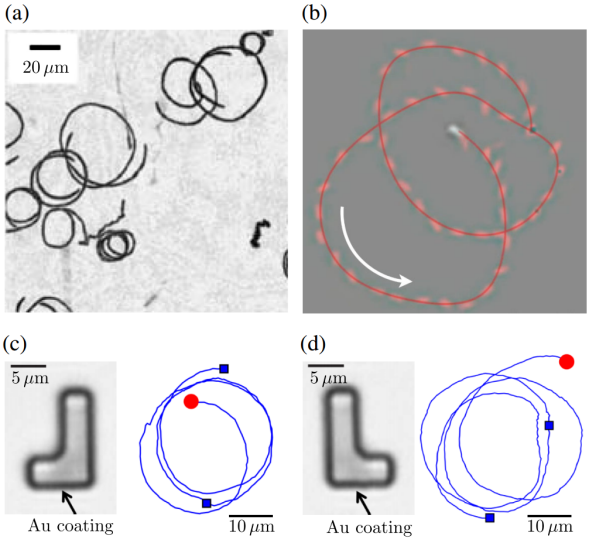

Figure 5: *(a): E. coli cells swimming in circular trajectories near a glass surface. Superposition of 8-s video images.[27] (b): E. coli bacteria swimming over liquid-air interfaces. Direction is reversed.*[9] *(c) adn (d):artificial microswimmers driven by self-diffusiophoresis. The red points represent the initial positions and the two blue squares the position after 1 and 2 minutes. The arrow on te insets mark the coating on the L-shaped particles, which is not visible here. Picture by Kümmel et al., 2013.*[25]

1.4.2 Run and Tumble

All the dynamics described until now is completely deterministic and in order to simulate organic and biological agents, this approach is not always suitable. Rather useful is to consider the so called *Run and Tumble* dynam-

ics. It consists of two states, one in which the particle performs a straight motion (run), and one, where it performs a rotation (tumble). The two states happen independent from each other, meaning that when a rotation move is performed, the translational propulsion is deactivated. The tumbling event consists of a randomly applied torque resulting in a rotation by an angle $\omega \in [-\pi, \pi]$ if the particle is free to rotate. The traveled distance between every tumbling event follows an exponential distribution $e^{-\nu t}$, since the the tumbling events happen at random times. This leads to a Poisson distributed number of rotating events per unit time, with mean frequency ν. The effective frequency $\nu_{eff} = \nu/(1 + \nu\tau_{tb})$ is commonly used, because a frequency considering ν alone does not allow for the fixed duration τ_{tb} of the tumbling event.

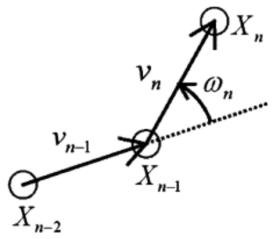

Figure 6: *Schematic run and tumble motion: The circles represent the run and tumble particle at positions X. Between the straight translational moves v_{n-1} and v_n, the tumbling move around the angle ω_n takes place. Picture by Yukio Magariyama et al., Biophysical journal 88.5 (2005).*[28]

The rotational diffusion coefficient of a single free swimming particle is

$$D_r = \nu_{eff} \frac{(2\omega)^2}{12}, \tag{15}$$

where $(2\omega)^2/12$ is the mean square angle, since the angle is evenly distributed in [-ω,ω]. The difference between the model for run and tumble particles as compared to the models used for active Brownian motion is crucial. While run and tumble dynamics consists of the 2 states explained above, for active Brownian particles rotational noise and self-propulsion are both constantly present.

An interesting example of possible behaviour differences between active Brownian and run and tumble particles is shown by Maryam Khatami et al.[23] When both are sent into mazes of different geometry, they show large differences in their stationary probability distributions. In particular, run-and-tumble particles enter the maze and easily move towards the center, while active Brownian particles escape faster towards the rim. In a steady state, persistent ABPs (Active Brownian Particles) accumulate in the outermost region of the maze, while RTPs (Run and Tumble Particles) spread more uniformly in all regions. This is due to the random walk, performed by the ABPs along the maze walls, allowing them to readily find openings in the wall, whereas, the dynamics of RTPs detaches the particles from the walls and therefore lowers the probability for them to find an opening. This peculiar phenomenon is more pronounced in mazes with curved boundaries.

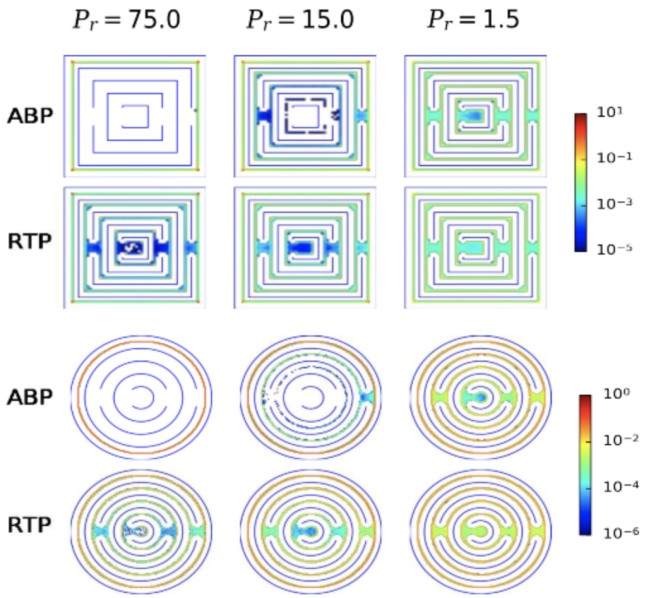

Figure 7: *Stationary distribution of active particles inside suare and circular mazes. P_r is the persistance number, which is the persistance length in units of the swimmer diameter. Picture by Maryam Khatami et al., Scientific reports 6 (2016).*[23]

1.5 Diffusion

For the study of dynamic properties of particles, the translational and rotational diffusion coefficient is of decisive importance. Especially for active particles, the dependence of those coefficients on parameters like particle density, as well as their dependence on each other[1], are yet to be intensly studied.

If we consider a given trajectory $\{r(t), p(t)\}$ at which one can measure the observables $A(r(t), p(t))$ and $B(r(t), p(t))$, one can give the time correlation function C_{AB} as a time average,

$$C_{AB}(t) = \frac{1}{\tau} \int_0^\tau A(s)B(s+t)\,\mathrm{d}s, \tag{16}$$

which we will denote as $C_{AB}(t) = \langle A(s)B(s+t)\rangle$. For a stationary state, the correlation can only depend on the time difference t, so we can write:

$$C_{AB}(t) = \langle A(0)B(t)\rangle. \tag{17}$$

The time correlation functions are simply connected to transport coefficients like the translational diffusion coefficient, which can be written as the autocorrelation of the velocity,

$$D = \frac{1}{3} \int_0^\infty \langle \mathbf{v}(0)\mathbf{v}(t)\rangle\,\mathrm{d}t. \tag{18}$$

A better approach for computational physics is to compute the diffusion coefficient with the *mean square displacement* (msd), which describes how fast a particle diffuses, e.g. how fast a particle moves away from a fixed point in space. Note that this calculation is valid for a long-time-limit only.

$$\lim_{t\to\infty} msd(t) = \lim_{t\to\infty} \frac{1}{N} \sum_{i=1}^{N} |\mathbf{r}_i(t-t_0) - \mathbf{r}_i(t_0)|^2 = 2dDt. \tag{19}$$

Here, $\mathbf{r}_i(t)$ is the position of particle i at time t, and d is the dimension of the space. Again, this is the translational diffusion coefficient. Typically, the msd for active Brownians initially increases quadratically in time, called

[1] See coupling of angle and position in equations (11)

the *ballistic regime*. Ater some time τ_B, it shows a crossover to the *diffusive regime*, where it gets linearly dependend.

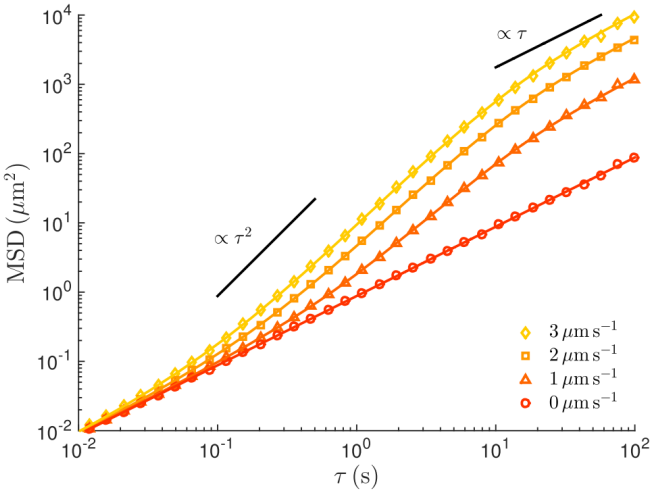

Figure 8: *Mean square displacement of an active brownian particle for different velocities: $v = 0\mu ms^{-1}$ (circles), $v = 1\mu ms^{-1}$ (triangles), $v = 2\mu ms^{-1}$ (squares), $v = 3\mu ms^{-1}$ (diamonds).* Picture by Bechinger et al., 2016.[3]

In the figure above, one can nicely see the transition from the ballistic to the diffusive regime. While for a passive Brownian particle the motion ($v = 0\mu ms^{-1}$) is always diffusive, dor active Brownians it is diffsuive at very short time scales $\tau \ll \tau_B$ with diffusion coefficient D_t from equation (8), then translates into the ballistic regime with quadratic dependence on *tau* for intermediate time scales $\tau \approx \tau_B$. It then goes to a diffusive regime again for scales $\tau \gg \tau_B$, but this time with an enhanced diffusion coefficient.

1.6 Self-propulsion mechanisms

The driving force which makes a particle self propelled can be not only of natural, but also of artificial origin like for the mentioned Janus particles. These particles are coated with different materials on each side, creating a net force due to the reactions of the sides with their environment. Applied examples are polystyrene spheres with a platinum cap placed in a hydrogen peroxide solution, where the platinum catalyzes the local decomposition of hydrogen peroxide into water and oxygen. The resulting asymmetric distribution of reaction products propels the particle by self-diffusiophoresis. During this process, gas is created, inducing another propulsion mechanism called *bubble-propulsion*. The creation and release of gas bubbles gives rise to the driving force on the coated particle. Although self-diffusiophoresis is the primary motor for platinum covered polystyrene spheres, bubble recoil can cause velocities as high as 1mm/s that is enough to overcome the background fluid flow in blood vessels[46]. Janus particles can be formed as spheres or rods, but are not limited to those shapes. Especially in the design of micromotors, asymmetrical shapes are more frequent[53, 49]. The examples given here are presenting just two possible ways of creating micromotor propulsion, others are self-electrophoresis[30], magnetic fields[39], the Marangoni effect[12] and enzymatic reactions[44]. All of them are nowadays studied intensively to enhance our understanding and advance the field of active matter.

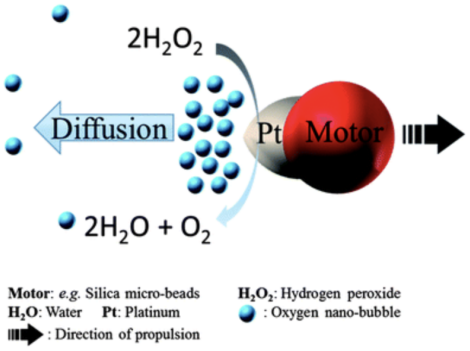

Figure 9: *Schematic representation of a nano-motor moving under the diffusiophoresis propulsion mechanism. Picture by Loai KEA Abdelmohsen et al., Journal of Materials Chemistry B 2.17 (2014).*[1]

1.7 Dipole interactions

For the research I performed in this work, along with active matter, it is essential to also discuss the behaviour of dipolar fluids, or ferrofluids, if they are exposed to an external field. An approximate model for the behaviour of such a bulk of dipoles considers them as hard spheres with point dipoles in the center. The interactions are then determined by the potential:

$$u_{dip}(r, \boldsymbol{\mu}_i, \boldsymbol{\mu}_j) = \frac{\boldsymbol{\mu}_i \cdot \boldsymbol{\mu}_j}{r^3} - \frac{3(\boldsymbol{\mu}_i \cdot \boldsymbol{r})(\boldsymbol{\mu}_j \cdot \boldsymbol{r})}{r^5}. \tag{20}$$

Here, $\boldsymbol{\mu}_i$ is the magnetic dipole moment vector of the i-th particle , r denotes the length of the displacement vector $\boldsymbol{r}$ between particles i and j. When all dipoles are coaligned with an externally applied strong magnetic field, due to the Zeeman-effect, potential (20) changes to

$$u_{dip}(r, \theta) = k_B T \frac{\gamma}{2} \left(\frac{\sigma}{r}\right) \left(1 - 3cos^2\theta\right), \tag{21}$$

where σ is the particle diameter. θ is the angle enclosed between the vector of the magnetic field and the interparticle vector $\boldsymbol{r}$; γ for a magnetic field is

$$\gamma = \frac{\pi \alpha^2 \sigma^3 \mu_s |\mathbf{H}_{loc}|^2}{8 k_B T}. \tag{22}$$

Here $\alpha = (\mu_p - \mu_s) \,/\, (\mu_p + 2\mu_s)$ and $\mathbf{H}_{loc} = \mathbf{H} + \mathbf{H}_{dip}$ is the local magenetic field. This potential is limited to the simplified model of spheres of same size and with identical magnetic moments.

Dipolar systems were heavily investigated during the past years[5, 47], also by Antti-Pekka Hynninen and Marjolein Dijkstra[17], who explored a system of dipolar hard spheres with the potential,

$$u_{HS} = \begin{cases} \infty & \text{for } r < \sigma \\ 0 & \text{for } r \geqslant \sigma \end{cases} \tag{23}$$

as steric interactions, showing that the dipoles assemble into chains as seen in figures 10 and 11. They show a snapshot of a simulation of a dipolar hard-sphere system with a magnetic field in the z direction . The behaviour of chain formation is clearly seen in the smaller inlet in the lower figure.

This alignment appears in the parallel direction to the magnetic field in order to minimise the free energy arising from the field-dipole interaction,

$$u_f = -\boldsymbol{\mu} \cdot \boldsymbol{H}. \tag{24}$$

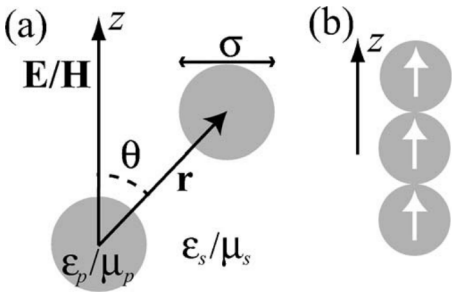

Figure 10: *(a): Dipole-Dipole interaction between two particles with diameter σ and magntic susceptibility μ_p. The solvent has a magnetic susceptibility μ_s. The vector of the magnetic field and the interparticle vector enclose an angle θ. In case of an electric field, the particles have a dielectric constant ϵ. (b): The dipoles (indicated by white arrows) favour positions where they are aligned head-to-toe. Picture by Antti-Pekka Hynninen and Marjolein Dijkstra, 2005*[17]

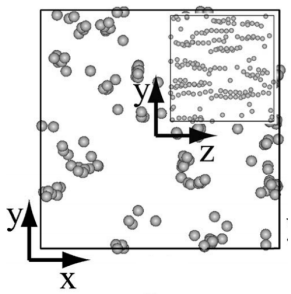

Figure 11: *Simulation snapshot of a dipolar hard-sphere system. Picture by Antti-Pekka Hynninen and Marjolein Dijkstra, 2005[17]*

If there is no field present, self-assembly is not restricted to the formation of chains. Especially for higher concentrations of magnetic particles, where the assumption of non interacting chains is not anymore defensable, one has to consider the formation of more complex structures such as rings, Y and X-shapes and eventually, networks. This has been shown by S. Kantorovich, A. Ivanov, et al., 2015[20], using Monte Carlo simulations and Density Functional Theory of dipolar hard sphere systems. The resulting formations are seen in figure 12.

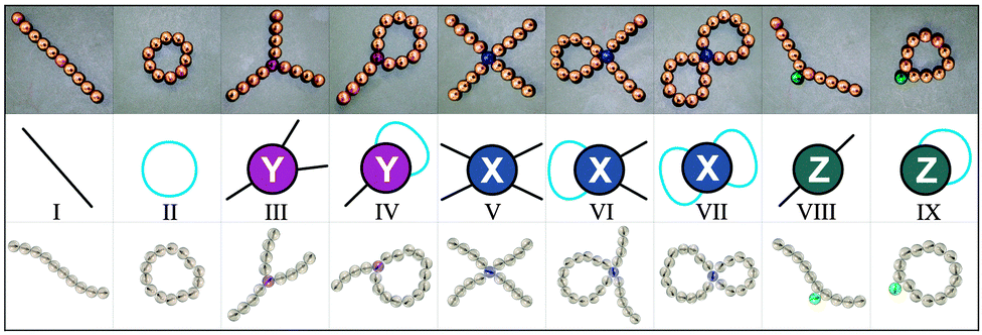

Figure 12: *Top row: photographs of commercially available magnetic beads; middle row: topological classification, here black indicates chain segments and blue - rings; bottom row: structures extracted from Monte Carlo computer simulations. Picture by S. Kantorovich, A. Ivanov, et al., 2015[20]*

In the model that we will use, steric interactions are governed by a transformation of the Lennard-Jones potential, which approximates the interaction between a pair of neutral atoms or molecules.

$$u_{LJ} = 4\epsilon \left[\left(\frac{\sigma}{r} \right)^{12} - \left(\frac{\sigma}{r} \right)^{6} \right]. \tag{25}$$

The transformation is realized by a shift that happens at the potential minimum at $r = \sqrt[6]{2}\sigma$, which cuts away the attractive part of the Lennard-Jones potential for $r \geqslant \sqrt[6]{2}\sigma$, making it purely repulsive. The resulting potential is called the *Weeks-Chandler-Andersen potential*,

$$u_{WCA} = \begin{cases} 0 & \text{for } r \geqslant \sqrt[6]{2}\sigma \\ u_{LJ} + \epsilon & \text{for } r < \sqrt[6]{2}\sigma \end{cases} \tag{26}$$

where ϵ is the depth of the potential-well.

1.8 Getting control over active systems

Taking into account the models and research introduced so far, I conclude shortly the interesting but also problematic properties of both, active and dipolar systems, if one wants to gain higher control over the systems motion.

Looking at active matter or active particles, it is immediately understood that the property of interest for research lies in the conversion of environmental to kinetic energy. One big advantage of this self-propulsion is that it can arise from a variety of mechanisms, providing many possibilities to scientists for its realization. A disadvantage of active matter systems, especially if their origin is of biological nature, is the difficulty to control and direct their motion, as they are in general, non magnetic and unaffected by fields.

Unlike active matter, dipolar particles are well controllable by applied fields. We see field induced chain and structure formation, which can be analyzed and quantified for better understanding of the system. The interesting property of active matter, self-propulsion, is lacking in these particles.

The work in my thesis aims at combining those two types of systems, taking the advantage of each to get an active matter system that can be influenced and, in the end, controlled by using dipolar particles and magnetic fields. The methods and ideas of how this is realized, are described in the following chapters.

2 Methods

2.1 Molecular Dynamics

Molecular dynamics (MD) simulations are a widely used technique to investigate the dynamics of classical many body systems, which means that it is made up by classical laws rather than quantum mechanical laws of physics. Though this already makes MD only an approximation, it is sufficient for a plethora of materials and systems. First, the system of interest is prepared in a microscopic state which is specified by the positions and momenta of all particles. This can be a state close to the systems equilibrium, but also far from it. Starting from this initial state, the Newton equation of motion

$$m_i \ddot{\vec{r}}_i = \vec{F}_i(r^N) \tag{27}$$

is solved for all N particles of the system in small time steps. This is commonly done using a finite difference approach, where the integrating algorithm should have the desired properties:

- It should be fast and require little memory
- It should allow the use of large time steps
- It should recreate the classical trajectory as closely as possible
- It should satisfy known conservation laws
- It should be simple to program

2.1.1 Velocity-Verlet

The most used algorithm for MD simulations is the *velocity verlet algorithm.* It can easily be derived by taking

$$\dot{x}(t) = v(t),$$
$$\dot{v}(t) = F(x(t))/m,$$

and using taylor expansions. First on $x(t + \Delta t)$:

$$x(t + \Delta t) = x(t) + \Delta t\dot{x}(t) + \frac{\Delta t^2}{2}\ddot{x}(t) + O(\Delta t^3).$$

By eliminating $\dot{x}$ with v and $\ddot{x}$ with F/m, we get:

$$x(t + \Delta t) = x(t) + \Delta t v(t) + \frac{\Delta t^2}{2}\frac{F(x(t))}{m} + O(\Delta t^3). \tag{28}$$

Then expanding $v(t + \Delta t)$,

$$v(t + \Delta t) = v(t) + \Delta t\dot{v}(t) + \frac{\Delta t^2}{2}\ddot{v}(t) + O(\Delta t^3),$$

and eliminating $\dot{v}$ with F/m and $\ddot{v}$ by expanding $\dot{v}(t)$, so we get:

$$v(t + \Delta t) = v(t) + \Delta t\dot{v}(t) + \frac{\Delta t}{2}(\dot{v}(t + \Delta t) - \dot{v}(t)) + O(\Delta t^3).$$

Finally, using the equation of motion, this can be rewritten as

$$v(t + \Delta t) = v(t) + \frac{\Delta t}{2m}(F(x(t + \Delta t)) + F(x(t))) + O(\Delta t^3). \tag{29}$$

The derived equations form the velocity verlet algorithm.

Velocity-Verlet integrator:

$$x(t + \Delta t) = x(t) + \Delta t v(t) + \frac{\Delta t^2}{2}\frac{F(x(t))}{m} + O(\Delta t^3);$$

$$v(t + \Delta t) = v(t) + \frac{\Delta t}{2m}(F(x(t + \Delta t)) + F(x(t))) + O(\Delta t^3).$$

Note that the velocities can only be computed after the new positions and hence the new forces are known. This integrating scheme has excellent energy conserving properties as it is phase space volume conserving[32]. Note also that a simulation can be run from initial conditions $\left\{r^N(0), p^N(0)\right\}$ and the scheme is therefore said to be "self-starting".

2.1.2 Langevin dynamics

What one would want to achieve if a simulation is to be made in an NVT-ensemble is constant temperature. To do so, it is not sufficient to integrate the Newton equations of motion, but rather the Langevin equation that was already shown in equation (5). The random forces are used to affect particles motion and therefore control temperature. This method is called *Langevin thermostat*. We now have to find a new integrator for the new modified equation of motion. This was done by Eijden and Ciccotti[43]. We first write the Langevin equation in one dimension in a differential form:

$$dr(t) = v(t)dt, \tag{30}$$

$$dv(t) = f(r(t))dt + \gamma v(t)dt + \sigma dw(t). \tag{31}$$

The above equations show some differences to the Langevin equation already introduced. To be able to derive the algorithm needed, the force term $-\nabla U/m$ is simply written as $f(r(t))$ and σ is $\sqrt{2k_bT\gamma/m}$, but the random forces have to be considered specifically. The random forces $F(t)$ can not be differentiated and they are therefore written as the integrals of a process $w(t)$ such that $F(t) = dw/dt$. Those processes are called *Wiener processes* with the main property:

$$\langle w(s)w(s')\rangle = \int_0^s \int_0^{s'} \langle F(t)F(t')\rangle dtdt' = \int_0^s \int_0^{s'} \delta(t'-t)dtdt' = min(s,s'). \tag{32}$$

Wiener processes are discussed by Karatzas, Ioannis, and Steven Shreve[21], but are not further handled here. By integrating equations (30) and (31) from t to $t + \Delta t$, you get

$$r(t+\Delta t) = r(t) + \int_t^{t+\Delta t} v(s)ds, \tag{33}$$

$$v(t+\Delta t)+v(t)+\int_t^{t+\Delta t} f(r(s))ds-\gamma\int_t^{t+\Delta t} v(s)ds+\sigma[w(t+\Delta t)-w(t)]. \tag{34}$$

Starting with the velocity integral that occurs in both equations, we use the lowest order

$$v(s) \approx v(t) + (s-t)f(r(t)) - (s-t)\gamma v(t) + \sigma[w(s) - w(t)],$$

where $t \leqslant s \leqslant t + \Delta t$, to get

$$\int_t^{t+\Delta t} v(s)ds = \Delta t v(t) + \underbrace{\frac{\Delta t^2}{2}[f(r(t)) - \gamma v(t)] + \sigma \int_t^{t+\Delta t} [w(s) - w(t)]ds}_{C(t)}. \tag{35}$$

We have now found an approximation for the velocity integral in (33) and (34). The force integral in the latter, is computed in a similar fashion using

$$\frac{df}{dt} = \frac{\partial f}{\partial r}\dot{r} = \frac{\partial f}{\partial r}v$$

to get

$$f(r(s)) = f(r(t)) + \int_t^s v(y)f'(r(y))dy \approx f(r(t)) + (s-t)v(t)f'(r(t)).$$

Again, like the velocity integral, we integrate from t to $t + \Delta t$:

$$\int_t^{t+\Delta t} f(r(s))ds = \Delta t f(r(t)) + \frac{\Delta t^2}{2}v(t)f'(r(t)) = \Delta t \frac{f(r(t + \Delta t + f(r(t))}{2}, \tag{36}$$

where the derivative $f'(r(t))$ is replaced by the use of

$$f(r(t + \Delta t)) = f(r(t)) + f'(r(t))v(t)\Delta t.$$

As the force and velocity terms are integrated, the only terms left to consider are $w(t+\Delta t) - w(t)$ and $C(t)$. To do so, properties of the Wiener processes and functions are used. In order to save space in this chapter, the derivation

of those terms is found in Appendix A, which leads to

$$\int_t^{t+\Delta t}(w(s)-w(t))ds = \Delta t^{3/2}\left(\frac{\xi}{\sqrt{3}}+\frac{\theta}{2\sqrt{3}}\right), \tag{37}$$

where ξ and θ are two uncorrelated random numbers. Plugging back in the derived approximations for the integrals in equations (33) and (34) we obtain

Integrator for the Langevin equation (second order):

$$r(t+\Delta t) = r(t) + \Delta t v(t) + C(t);$$

$$v(t+\Delta t) = v(t) + \frac{\Delta t}{2}[f(r(t+\Delta t)) + f(r(t))] - \Delta t\gamma v(t) + \sigma\sqrt{\Delta t}\xi(t) - \gamma c(t);$$

$$c(t) = \frac{\Delta t}{2}[f(r(t)) - \gamma v(t)] + \sigma\Delta t^{3/2}\left(\frac{\xi}{\sqrt{3}}+\frac{\theta}{2\sqrt{3}}\right).$$

If γ and σ are both set to be 0, this scheme becomes the already discussed Velocity-Verlet integrator.

2.1.3 Force calculation

Typically, the computation of the forces is the most time consuming part in an MD simulation. In the absence of a magnetic field, the force $\boldsymbol{F}_i$ on particle i is given by the negative gradient of the potential energy $U(r^N)$:

$$\boldsymbol{F}_i = -\boldsymbol{\nabla}_i U(r^N), \tag{38}$$

where $U(r^N)$ is in general a complex function of particle coordinates. While for atomistic systems the potential energy arises from the solution of Schrödinger equation, for a pairwise additive potential, the force calculation becomes an easier task, as the potential energy can be written as a sum:

$$U(r^N) = \sum_{i<j} u(t_{ij}), \tag{39}$$

where r_{ij} is the distance between the i-th and the j-th particle. The force on a particle is then given by:

$$\boldsymbol{F}_i = -\boldsymbol{\nabla}_i U(r^N) = \sum_{j \neq i} \boldsymbol{f}_{ij}, \tag{40}$$

where

$$\boldsymbol{f}_{ij} = \frac{\partial u(r_{ij})}{\partial r_{ij}} \frac{\boldsymbol{r}_{ij}}{r_{ij}} \tag{41}$$

is the force experienced on an particle j by an particle i. From the pairwise additive nature of the potential follows that

$$\boldsymbol{f}_{ij} = -\boldsymbol{f}_{ij}.$$

Although the use of pairwise additive potentials simplifies the force calculation, there is still the need to compute $N(N-1)/2$ pair distances. Hence, the computational cost of a full force calculation scales with N^2. In order to keep the the computational cost reasonably low for larger N, one can make use of some tricks that reduce the effort to a linear scaling. They can be used for short-range interaction potentials (interactions that decay faster than $1/r^2$). I describe some of these tricks below.

2.1.4 Verlet lists

As there is a cutoff r_c used for the pairwise additive potential, most pairs of atoms do not contribute to the total potential energy, especially if one simulates large systems. It is now advantageous to drop the force calculation for those pairs in order to save computing time. This can be achieved by utilising *verlet lists* or *neighbour lists*. For that, a new cutoff $r_l > r_c$ is introduced. For each particle i, a list is created that contains all particles within r_l from this particle i. Then, only particles in this list have to be considered for the force calculation. Since for the calculation of the lists one has to loop over all particle pairs, it results again in N^2 scaling, but once this has been done the force evaluation scales linearly.

The method of Verlet lists is only of advantage if the lists do not have to

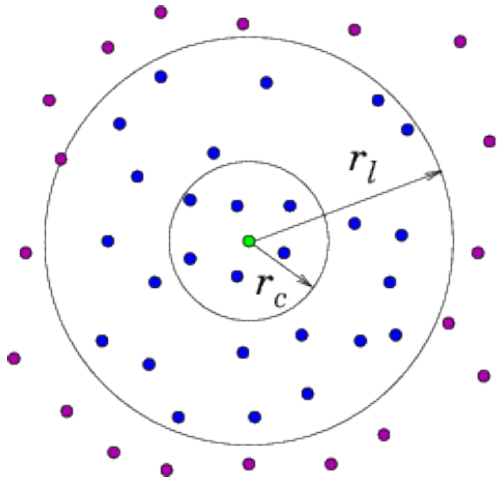

Figure 13: *Schematic idea behind Verlet lists.* r_c *is the cutoff of the potential and* r_l *the newly introduced cutoff used for the verlet list creation. The distances from the green to all blue particles are computed, the purple ones are neglected. Picture by Massachusetts Institute of Technology.*

be recomputed at every time step. Thus, r_l has to be chosen appropriately, since a recalculation of the lists needs to take place if a particle moves further than the distance $r_l - r_c$. Although the computation of the lists only happens every couple of time steps, it becomes the most significant factor for the computational cost.

2.1.5 Cell lists

Another trick is not to construct lists for every particle in the system, but to create a list of particles in a certain region of space. This is called the *cell list method* or *linked list method*. The simulation box is divided into cells with sides a bit larger than r_c and for each cell a list is constructed, which contains all particles within the given cell. As the side length of the cells is chosen to be bigger than the cutoff, a particle only interacts with particles in its own, or its neighbouring cells. This scales the force computation down to the order of N. A combination of both, verlet and cell lists, is possible and of advantage.

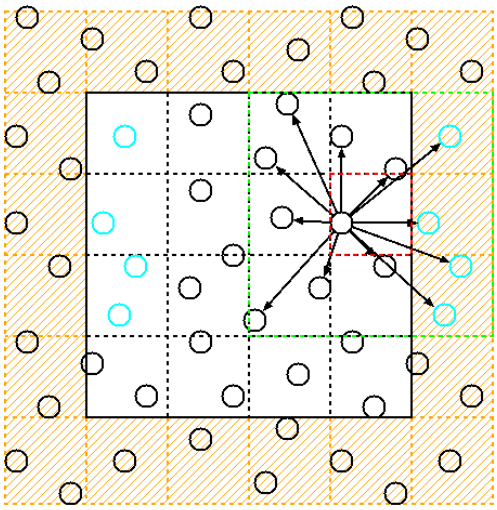

Figure 14: *Schematic idea behind cell lists. The orange shaded cells indicate the periodic pictures of the simulation space which are used with periodic boundary conditions. Picture by Pedro Gonnet[11].*

2.1.6 Instability

Our goal with making an MD simulation, is to model the dynamics of particles in our chosen system. Starting from some initial condition $x_0 = \left\{r^N(0), p^N(0)\right\}$, we solve the equations of motion producing a trajectory $x_{i\Delta t} = \left\{r^N(0)_{i\Delta t}, p^N(0)_{i\Delta t}\right\}$ that consists of points in phase space. Is it realistic that this trajectory mimics the true trajectory of the real system? As it turns out, it is impossible to follow a systems real dynamics, especially for long time scales. This fact is part of the chaos theory. A system of differential equations is said to be chaotic, if its dynamics is highly sensitive to small changes in the initial conditions. So if a system is chaotic, such small changes will lead to a completely different time evolution for longer time scales. What does this imply for MD? We consider an exact trajectory $x_t(x_0)$ with initial conditions x_0. If we now displace these conditions by a small amount $\delta_0 = \left\{\delta r^N(0), \delta p^N(0)\right\}$, we get the exact trajectory $x\prime_t = x_t + \delta_t$. For many systems, the displacement $\delta_{x_t} = x\prime_t - x_t$ grows exponentially:

$$\mid \delta_{x_t} \mid \sim \mid \delta_{x_0} \mid e^{\lambda t}, \tag{42}$$

which means that the initially close trajectories quickly start to diverge. λ is

called the *Lyapunov exponent* and in 3 dimensions, there are $6N$ exponents.

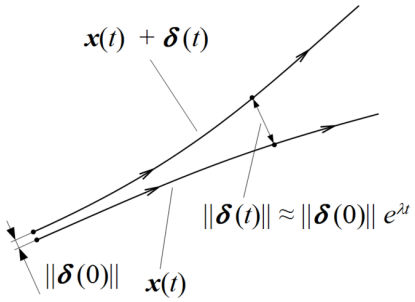

Figure 15: *Deviation of trajectories with different initial conditions*

This seems dramatic at first, as we just learned that it is not possible to know the true dynamics of a system, but as we are interested in statistical measures such as correlation functions and we also only know the statistical distribution of initial conditions, MD simulations are still a powerful tool in computational science.

2.1.7 P^{3}M-Method

As already said, force computation is the most time consuming part of MD simulations. Especially expensive are long-range magnetostatic or electrostatic interactions, such as, for example, forces introduced in section 1.7. Using lists and/or cut-offs for such potentials might lead to serious errors, but direct methods are also very costly. It is therefore useful to use an enhanced algorithm for their computation. An example for such a procedure is the P^3M-Method (Particle-Particle/Particle-Mesh)[6]. It combines two ways to sum magnetostatic forces. The first is the simple Particle/Particle-Method (PP), which is the brute-force approach as it sums over all pairs of particles. A desired feature of PP, is that no sum is in any way approximated, and its accuracy is limited only by machine precision. Unfortunately, PP is not feasible for large numbers of particles due to its scaling behaviour of N^2. The second is the Particle-Mesh-Method (PM). The main idea is to discretize space and to solve the Poisson equation

$$\nabla^2 \Phi = c\rho;$$

$$U = \nabla \Phi,$$

on the applied grid (mesh) of the discretization. The forces of the grid points can be calculated by taking the gradient of the potential U. The forces not located at grid points are computed as the interpolation to the closest grid point, or simply as the force at the grid point itself.

In order to solve the Poisson equation, the density function ρ (in the case of magnetostatics, ρ is the dipole density), must be determined. This can be achieved in different ways:

- **Nearest gridpoint:** The particle property is assigned to the gridpoint closest to the particle
- **Cloud-in-Cell:** The particle property is weighted over the closest surrounding cells (4 in 2D, 8 in 3D), with the weighting beeing proportional to the intersection of the "cloud" surrounding the particle and the cells.
- **Higher order interpolation:** The weighting function can be interpolated with higher orders, thus it is covering more cells.

After the density function is determined, the potential and therefore the forces can be computed. The weak spot of the PM is the constraint in space resolution, resulting in incorrect modelling of interactions smaller than the grid spacing. The P^3M-Method[6] combines the accuracy of PP at small ranges, with the efficiency of PM at bigger ranges.

In the case of dipolar interactions, the use of Ewald summation is of advantage[6]. It splits the dipolar pair interaction

$$u(r, \boldsymbol{\mu}_i, \boldsymbol{\mu}_j) = \frac{\boldsymbol{\mu}_i \cdot \boldsymbol{\mu}_j}{r^3} - \frac{3(\boldsymbol{\mu}_i \cdot \boldsymbol{r})(\boldsymbol{\mu}_j \cdot \boldsymbol{r})}{r^5},$$

shown in section (1.7) into two parts:

$$u(r, \boldsymbol{\mu}_i, \boldsymbol{\mu}_j) = (\boldsymbol{\mu}_i \cdot \nabla_{\boldsymbol{r}_i})(\boldsymbol{\mu}_j \cdot \nabla_{\boldsymbol{r}_j})(\psi(r) + \phi(r)). \tag{43}$$

Here $\psi(r)$ contains the short distance part of the Coulomb interaction and $\phi(r)$ contains its long distance part. There are multiple choices for the splitting functions[10, 16], but the standard way is to choose Gaussian functions:

$$\begin{aligned} \psi(r) &:= \frac{\operatorname{erfc}(\alpha r)}{r}; \\ \phi(r) &= \frac{\operatorname{erf}(\alpha r)}{r}, \end{aligned} \tag{44}$$

where *erf* and *erfc* are the error- and the complementary error function. The so called splitting or Ewald parameter α weights the importance of one term with respect to the other. This parameter can be chosen to optimize the performance of the method and automatic algorithms for this tuning are available.

The short ranged interactions are summed as already discussed in the PPM, but for computing the long ranged part, Fourier transforms bring significant acceleration to the method since long range interactions transform to short ranged interactions in Fourier space (k-space). The splitting of the potential leads to the well known Ewald-formula

$$U = U^{(r)} + U^{(k)} + U^{(\text{self})} + U^{(\text{surf})}, \tag{45}$$

with

$$\begin{aligned} U^{(r)} &= \frac{1}{2} \sum_{i,j=1}^{N} \sum_{\boldsymbol{n} \in \mathbb{Z}^3} (\boldsymbol{\mu}_i \cdot \nabla_{\boldsymbol{r}_i})(\boldsymbol{\mu}_j \cdot \nabla_{\boldsymbol{r}_j}) \psi(r); \\ U^{(k)} &= \frac{1}{2V} \sum_{\boldsymbol{k} \in \mathbb{K}^3} |\hat{\boldsymbol{\rho}}(k) \cdot i\boldsymbol{k}|^2 \hat{\phi}(\boldsymbol{k}); \\ U^{(\text{self})} &= -\frac{2\alpha^3}{3\sqrt{\pi}} \sum_{i_1}^{N} \mu_i^2; \\ U^{(\text{surf})} &= \frac{2\pi}{(2\epsilon+1)V} \sum_{i=1}^{1} \sum_{j=1}^{N} \boldsymbol{\mu}_i \cdot \boldsymbol{\mu}_j. \end{aligned} \tag{46}$$

Here V is the box volume and ϵ is the dielectric constant of the medium surrounding the replica boxes. The energies that contribute to the Ewald-

formula, are the real-space energy $U^{(r)}$, the reciprocal-space energy $U^{(k)}$, and the surface energy $U^{(\text{surf})}$. The quantities $\hat{\boldsymbol{\rho}}$ and $\hat{\phi}$ are the Fourier transforms of $\boldsymbol{\rho}$ and ϕ, respectively. The self energy $U^{(\text{self})}$ describes the interaction of a dipole with itself and is therefore undesired and subtracted from the total energy. For the forces, due to $U^{(\text{self})}$ and $U^{(\text{surf})}$ being particle position independent, follow:

$$\boldsymbol{F}_i = \boldsymbol{F}_i^{(r)} + \boldsymbol{F}_i^{(k)}. \tag{47}$$

The P^3M-Method uses Fast Fourier Transforms (FFT) instead of standard Fourier Transforms, as for example the dipolar Ewald summation, hence it reduces the computational operations from $N^{3/2}$ to $N \log N$. However, because the FFT is a mesh operation, the need to mesh all dipoles onto a grid and solving the Poisson equation builds a restriction the on speed of this method. A comparison of the force calculation speed between Ewald and P^3M Method is seen in figure 16.

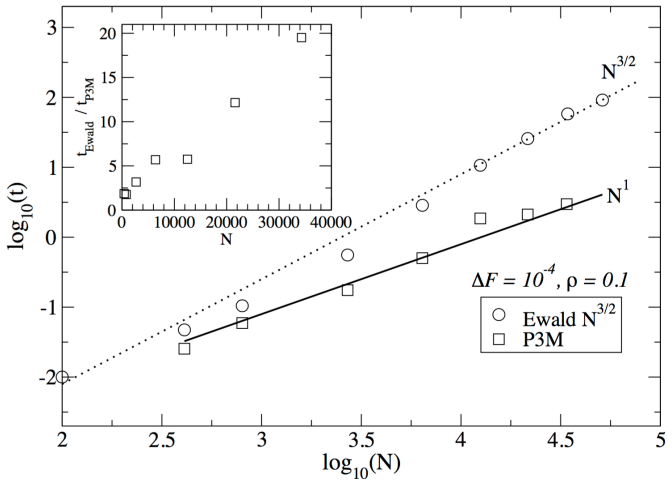

Figure 16: *Time taken for force and torque computation dependent on the number of particles. Circles represent the optimal dipolar Ewald-Method and squares the introduced P^3M-Method. The force accuracy is $\Delta F = 10^{-4}$ and both methods have optimal parameters for this value. The dipole density $N/V = 0.1$. The continuous and dotted lines have slope 1 and 3/2 respectively. Picture by Juan J. Cerda et al., "P3M algorithm for dipolar interactions" (2008).*

2.1.8 Reduced units

In molecular dynamics, we often find the Lennard-Jones potential introduced in section 1.7, as the prominent pair interaction potential. If this is the case, it is sensible to use a set of units, called *reduced units*, which are completely specified by the parameters ϵ and σ of the Lennard-Jones potential. This is achieved by using ϵ as a fundamental unit of energy and σ as a fundamental unit of length, so that for reduced physical quantities (usually marked with an "$*$" symbol) follows:

$$\begin{aligned} T^* &= k_B T/\epsilon && \text{Temperature} \\ E^* &= E/\epsilon && \text{Energy} \\ \rho^* &= \rho\sigma^3 && \text{Density} \\ \boldsymbol{f}^* &= \boldsymbol{f}\sigma/\epsilon && \text{Force} \\ \boldsymbol{t}^* &= \boldsymbol{t}/\epsilon && \text{Torque} \end{aligned}$$

and so on. The technical advantages of using reduced units appear, if σ and ϵ have been given a value of unity so they do not need to appear in a simulation at all, saving time on computing forces, energies etc.

2.2 Delaunay triangulation

A method used in the analysis part of this work is the *Delaunay triangulation*, named after Boris Delaunay for his work on this topic in 1934[8]. Triangulation, the decomposition of space into simple triangles, can be achieved in different forms. By defining the Delaunay condition, which states that for a given set of points, the circumcircle of every triangle resulting from the triangulation is empty, one gets the Delaunay triangulation. This property is also called "empty circle property".
Figure 17 shows an example for a Delaunay triangulation of 6 points in 2 dimensions. The solid circles show the circumcircles of the triangles resulting from the procedure, which are per Delaunay condition empty. The dashed circle shows a non empty circumcircle of a triangle span up by 3 points, thus, it is not usable for the final triangulation.

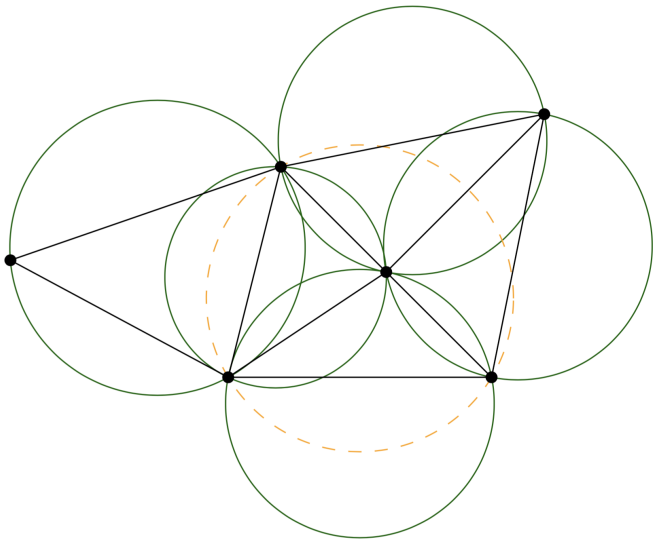

Figure 17: *Example for a Delauney triangulation of 6 points in 2 dimensions. Picture from lecture note "Theory of combinatoral algorithms", https://www.ethz.ch/de.html*

While the goal of a triangulation itself is not to have empty circumcircles, Delaunays method satisfies an interesting and useful property. The triangulation maximises the smallest angles, meaning that long and skinny triangles are unfavoured and appear less than in other triangulation methods. This leads to a more equiliteral triangle distribution which makes it widely used in computer science.

2.3 Active Brownian in ferromagnetic fluid

After having summarised essential facts concerning active particles and self assembly of magnetic nanoparticles in applied fields, I would describe the scenario implemented in my thesis. We consider a viscoelastic carrier fluid of dipolar particles and switch on a constant strong magnetic field. Due to minimization of the free energy, the dipoles will align with the field. The alignment of nanoparticle chains, as well a the increase of chain length, were predicted. Thus, the system becomes lightly anisotropic. The idea of my work is to place a generic non magnetic active Brownian particle in a solution of magnetic particles subjected to a strong field, and analyze its trajectory. Since the anisotropy of the system will heavily affect its motion, the expected outcome is that the active particle will move along the chains, as through the tunnels, once the magnetic field is switched on. To break the idea down to one sentence: *We want to control the motion of a non magnetic active Brownian particle, with a magnetic field using magnetic nanoparticles.*

2.3.1 ESPResSo

This scenario was investigated using molecular dynamic simulations, more specifically, using a molecular dynamics package called ESPResSo (Extensible Simulation Package for Research on Soft matter)[2].

This package was developed at the university of Mainz and solves the equations of motion for coarse grained modeled many body systems with the velocity Verlet algorithm. ESPResSo consists of two main parts. First the main code written in the C programming language, second the TCL (Tool Command Language) environment, that builds the bridge between user and computer. In order to set-up a simulation, one has to write a TCL script, using commands provided by ESPResSo. The script then gives control to the kernel, which executes the

commands and therefore runs the main simulation loops. A massively important feature of ESPResSo is its parallelization as it brings a significant boost to the simulation, especially for many particle systems. Therefore, the parallel version of ESPResSo was used for obtaining all results shown in this thesis.

2.3.2 Vienna Scientific Cluster

Since molecular dynamic simulations of many particle systems demands for large amounts of computational power, running it on a regular household PC would not be time efficient. Therefore, our simulations were executed on the *Vienna Scientific Cluster*, which consists of 3 units (VSC 1, VSC 2 and VSC 3). After installing ESPResSo on the cluster, jobs could be uploaded, which are then queued in to a waiting list and eventually executed.

2.4 Set-up

To simulate the active particle in a bath of magnetic nanoparticles described above, we set up a cubic simulation box. In my work I only use NVT-ensembles. Among N magnetic particles, there is one active Brownian particle which has a constant velocity. For all simulations, periodic boundary conditions were included in all directions. From this arises an important constraint for the size of the simulation box. While the active particle travels through the ferromagnetic fluid, it pushes away the magnetic particles due to the steric interactions. Especially in higher density fluids, this leads to the formation of tunnels created by the active particle itself. This effect will result in unphysical data, if the simulation box is chosen to be too small and the active particle builds tunnels for its periodic self. It is, therefore, a necessity to choose a box size that prevents this unwanted effect.

All particles interact according to the Week-Chandler-Andersen potential seen in equation (26), which is a pairwise additive potential and therefore fairly straightforward to compute. Verlet lists and cell lists as described in sections 2.1.4 and 2.1.5 are used to keep the computational cost at a minimum. The dipole-dipole interactions are computed according to equation

(20), utilising the P^3M method. A workflow chart of the simulation is seen in the figure below.

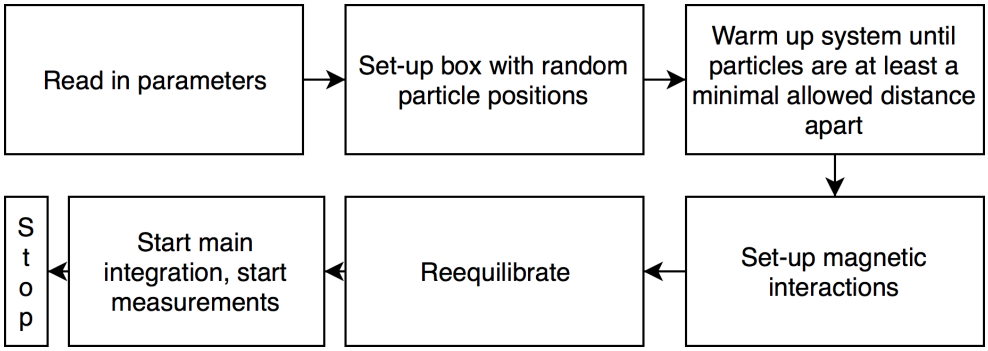

Figure 18: *Workflow-chart of the simulation script*

Before the script is executed, it is necessary to give various parameters such as particle numbers, magnetic moment, magnetic field strength, temperature and velocity of the active particle. All parameters are quantitatively given in the result section 3, as for now I will describe the general scheme of the simulation set-up. The script first places the particles on random locations inside the box. The density of the fluid is given as a dimensionless number density $\rho_d^* = N\pi\sigma_{dd}^3/6V$, where σ_{dd} is the magnetic bead diameter. The next crucial step is to warm-up the system. Due to the random locations that are given to all particles, the probability arises that two of them overlap and the highly repulsive force resulting from the Weeks-Chandler-Andersen potential at small distances would then "shoot them out" of the box. This is solved, by first integrating the equations of motions with a much smaller time step than for production integration. Additionally, a "force cap" is applied to the potential, setting the potential to be constant below a certain distance, which prevents the repulsive forces from becoming too big during equilibration. The warm-up stops when a minimum distance between the particles is reached. After the first warm-up, magnetic interactions and the magnetic field is turned on. Then equilibration is executed again. At this point ,the alignment of the dipoles happen, which can be seen in the simulation snapshot in figures 19 and 20 below.

Production integration is started after the second equilibration. At this point, until the end of the simulation, the position of the active particle is saved for further analysis. The simulation must run at constant temperature, so a Langevin thermostat is used to take energy from the system and therefore keep the temperature constant. With the collected data the *Mean Square Displacement* as seen in equation (19) is calculated for every spatial direction.

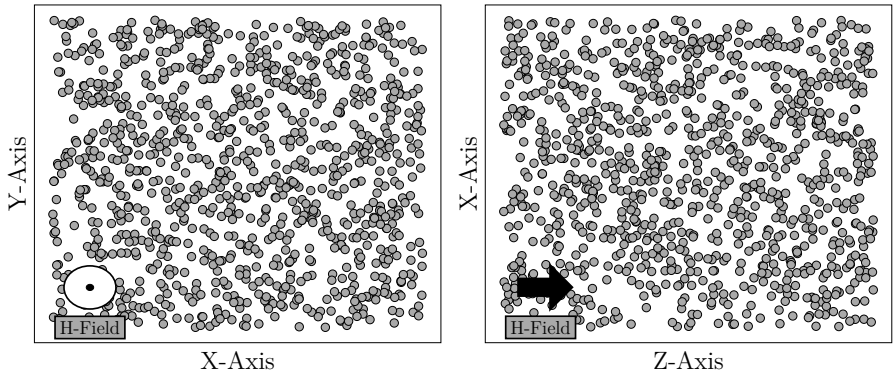

(a) x-y plane (b) z-x plane

Figure 19: *Unaligned: 2D projected simulation snapshot of only the magnetic fluid (without active particle) before the equilibration with an applied magnetic field. In (a) the field is directed into the plane, in (b) its directed from left to right.*

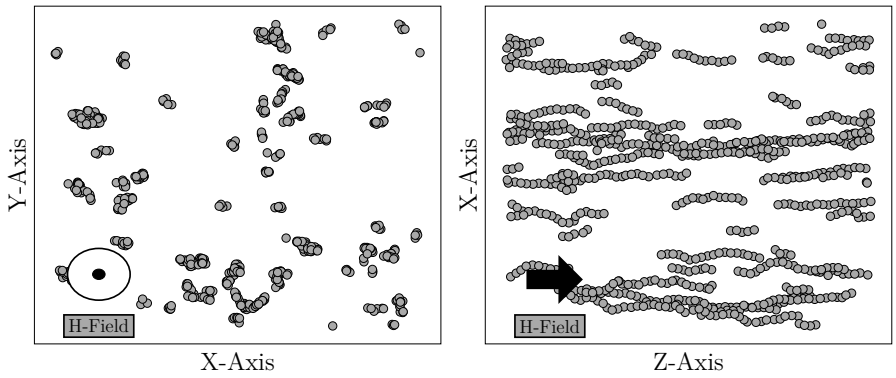

(a) x-y plane (b) z-x plane

Figure 20: *Aligned: 2D projected simulation snapshot of only the magnetic fluid (without active particle) after the equilibration with an applied magnetic field. In (a) the field is directed into the plane, in (b) its directed from left to right.*

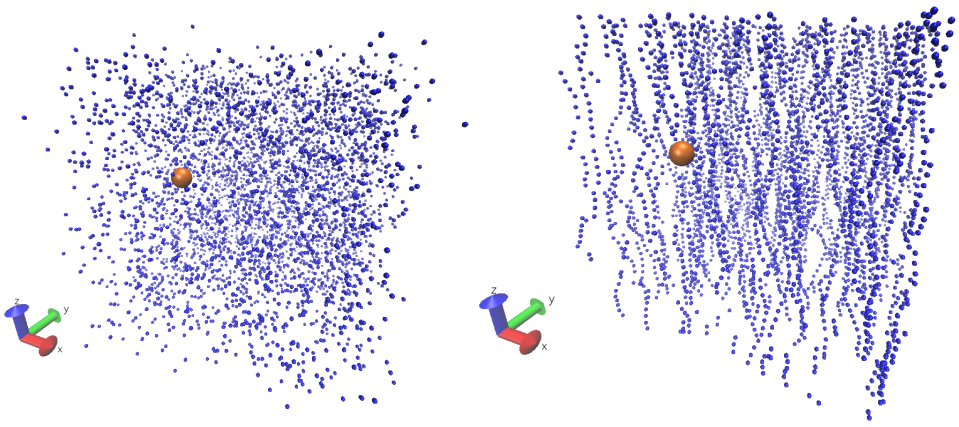

(a) Unaligned (b) Aligned

Figure 21: *3D simulation snapshots before (a) and after (b) equilibrating the system with magnetic interactions turned on. The blue dots represent the dipoles that build chains under the presence of a magnetic field (b). The red particle represents the active Brownian particle. The magnetic field is constant in the z-direction (blue arrow).*

3 Results

The first qualitative analysis of the system can be done on the ferrofluid without the inserted active particle. The ferrofluid shows the behaviour of self-assembling in chains (figures 19, 20 and 21) as explained in section (1.7) for dipolar hard spheres. Knowing the properties of this environment, the following section presents the results obtained from molecular dynamic simulations including the active particle inside a bath of magnetic particles. All units displayed, are dimensionless reduced units, which are marked with a symbol "*" above the respected quantity, where the unit length is the Lennard-Jones sigma σ_{dd} from the steric dipole interaction and the energy unit is ϵ=1 . For all simulations employed to obtain the following results, these parameters were used:

$T^* = 1$	Temperature
$\mu^{2*} = 5$	Magnetic moment of ferroparticles
$v^* = 2$	Velocity of active particle
$H_z^* = 3$	Magnetic field along z-axis
$r_D^* = 0.5$	Radius of the magnetic beads
$m_D^* = 1$	Mass of the magnetic beads

3.1 Size ratio 1:5

Although we investigate generic active particles, it would be useless to look at systems where the active particle has unphysical sizes compared to the magnetic nanoparticles, hence for example the same size. The reduced value for the magnetic bead size approximately corresponds to, for example, magnetite particles with a 20nm diameter. Therefore, the lower border for this system to be physical is a ratio of 1 to 5 between the size of the magnetic and the size of the active particle, where the mass ratio is 1 to 25[3].

The main measure taken from the system, is the mean square displacement of the active particle. This and the resulting diffusion coefficient can

be seen in figure 21. For all following MSD and diffusion coefficient plots, colors represent different ferrofluid number-densities ρ_d^* which are marked in the legend. Solid lines show the displacement parallel to the magnetic field (z-direction) and dashed lines the mean of the perpendicular directional displacements ((x+y)/2).

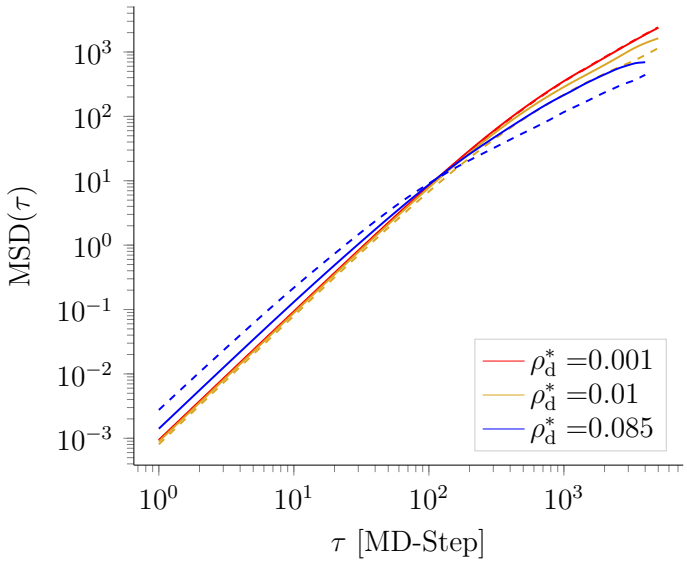

(a) Mean-Square-Displacement

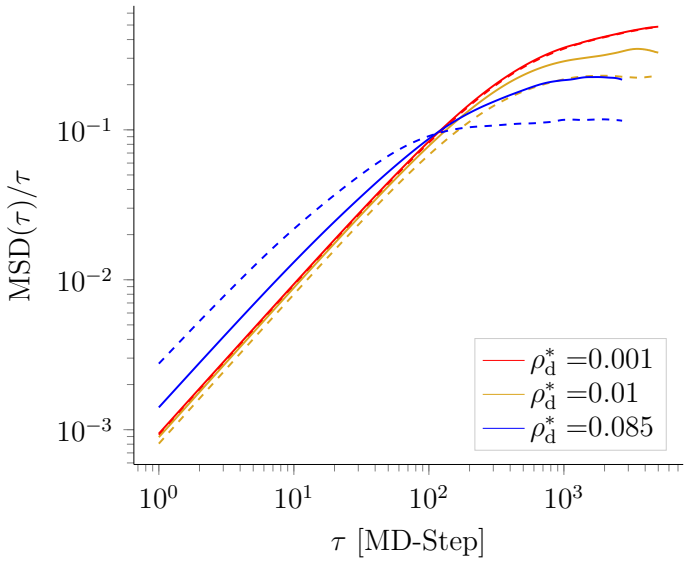

(b) Diffusion Coefficient

Figure 22: *Mean-Square-Displacement (a) and diffusion coefficient (b) for a dipole to active particle size ratio of 1:5.*

There it is seen, that the mean square displacement for the spatial direction perpendicular and parallel to the applied magnetic field shows significant deviations from each other. This becomes clearly visible in the relaxed regime, starting at $\tau \approx 10^2$ for ρ_d^* =0.085, above the ballistic part of the curve and indicates that diffusion is not the same in every direction like it is for a free active particle. Furthermore, it is noticeable that this said difference varies for changing number-densities ρ_d^* of the ferromagnetic particles.

Why does this system behave like that? To find the answer, one has to take a closer look at the environment the active particle finds itself in. The path it will take is determined by the space not occupied by magnetic particles. Since the latter form chains and therefore effective tunnels, a measure of interest is the width of those tunnels, or in general the space between the formed chains. This can be realized by taking all the chains in a snapshot of the simulation (leaving out single particles or chains of length 2 and 3, as they do not considerably contribute to directing the active particle) and look at the particles in single x-y planes. By triangulation of the resulting 2 dimensional projection of particles, one can find the space in between the chains. The results of this calculation are shown in figure 23 and 24. It was done by applying the Delaunay-triangulation method to several x-y planes of multiple snapshots. To increase statistical accuracy, the 8 nearest periodic images of the simulation box were taken into account . Error bars result from averaging over many x-y planes in different snapshots, and the histogram bin uncertainty.

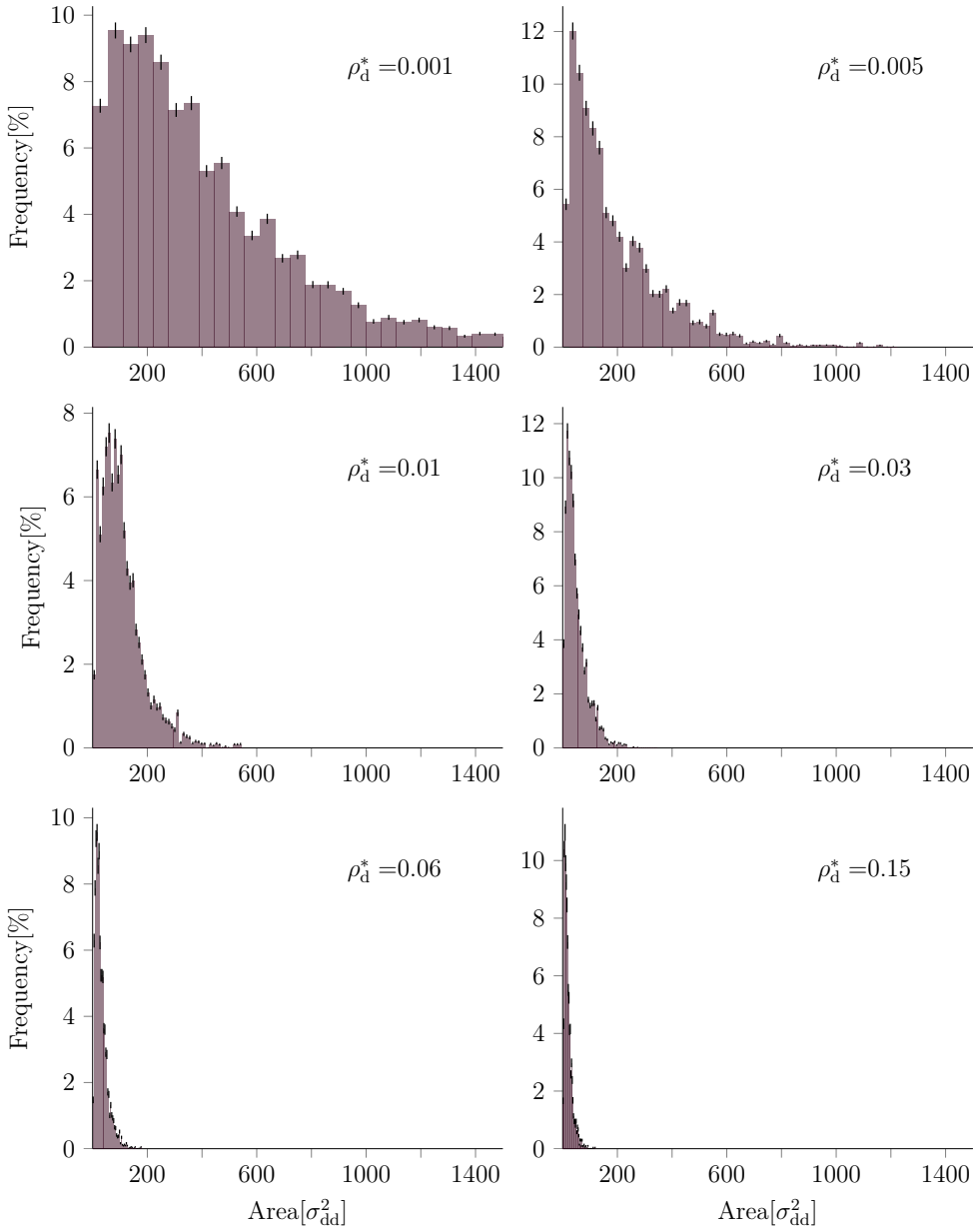

Figure 23: *Distribution of areas of the triangles resulting from triangulating dipoles that are in the same x-y plane. Each graph shows the distribution for a different ρ_d^* (increasing from top left to bottom right).*

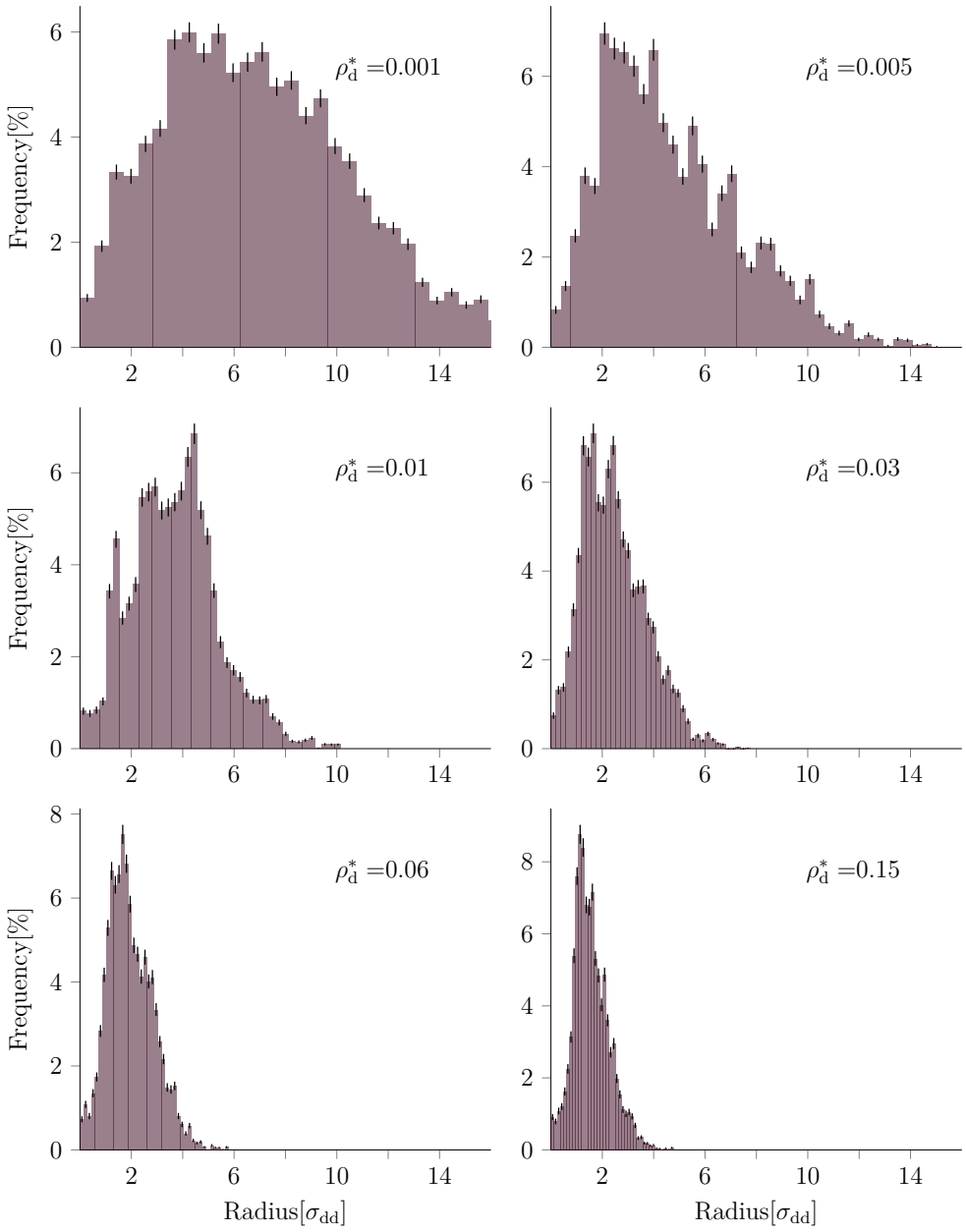

Figure 24: *Distribution of radii of the inscribed circles resulting from triangulating dipoles that are in the same x-y plane. Each graph shows the distribution for a different ρ_d^* (increasing from top left to bottom right).*

The two distributions in figures 23 and 24 show the triangle areas and the inscribed circle radii, for ferrofluid number-densities ranging from ρ_d^*=0.001 to ρ_d^*=0.15. Both distributions drastically shift to smaller sizes with increasing densities, meaning that the active particle gets trapped between the chains at higher densities. This fact and the already mentioned difference of spatial diffusion, suggests the following idea. For low densities, the active particle can move rather freely through the box, as it is not substantially directed by the alignment of magnetic particles into any direction. For very high densities, the chains are too close to each other and do not allow the diffusion of the active particle in any direction as it gets trapped inside the dense fluid. In between those two scenarios, there should be a case in which the active particle is blocked from moving in the x-y plane, but can still travel through the effective tunnels formed along the magnetic field direction. It, therefore, becomes interesting to look at the ratio of the diffusion parallel and perpendicular to the field direction. This measure is displayed for a range of ferrofluid number-densities in figure 25. Error bars for this measure result from time averages by splitting the simulation runs into equally sized parts, computing the measure for each part individually. It is clearly seen, that the efficiency for the transport strongly depends on the environmental density and peaks at ρ_d^*=0.08 for a 1:5 particle size ratio. As it has been already discussed, this arises from the limited freedom of space the swimmer experiences at higher densities. This further suggests, that different size ratios should be investigated as the space which allows a bigger active particle to move freely must shift to lower densities of its surrounding. Therefore, the same measures as above are now presented for a magnetic to active particle size ratios of 1:7 (mass ratio 1:70) and 1:10 (mass ratio 1:200).

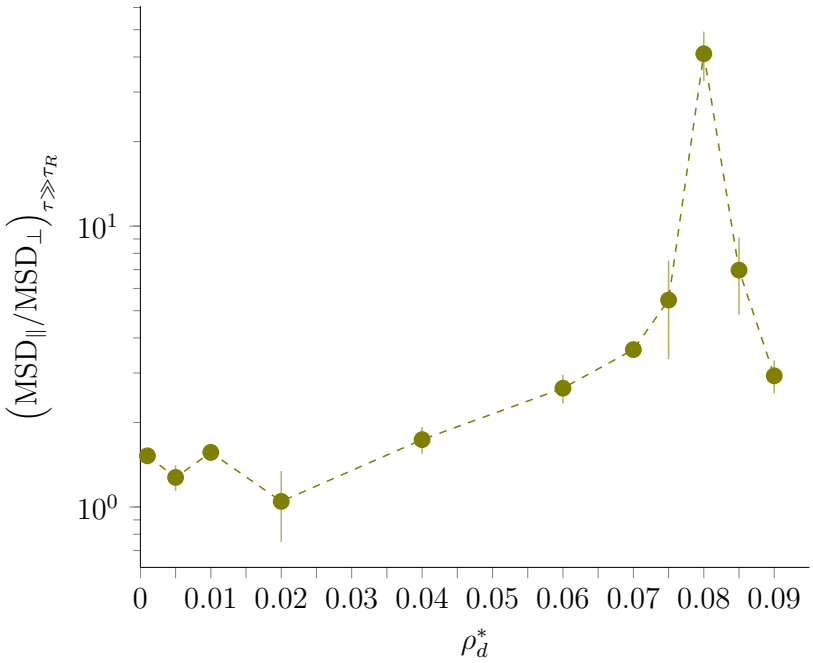

Figure 25: *Ratio of parallel to perpendicular diffusion, with respect to the applied magnetic field, at times much bigger than the relaxation time τ_r for a magnetic to active particle size ratio of 1:5. The peak efficiency occurs for $\rho_d^* = 0.08$ ferrofluid number-density.*

3.2 Size ratio 1:7

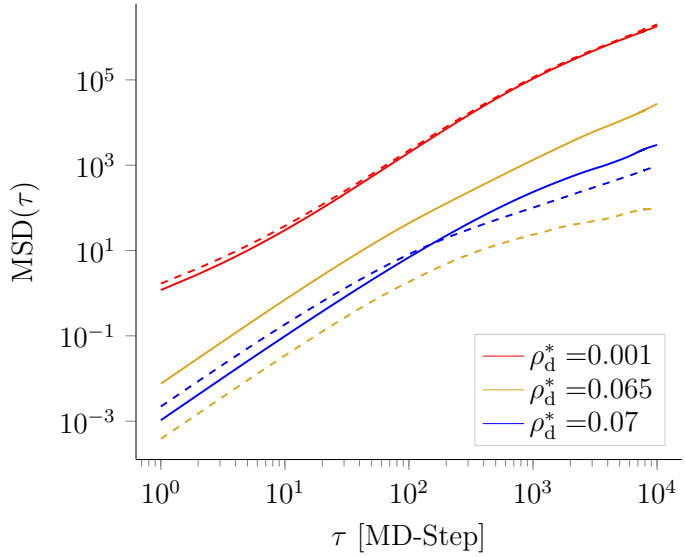

(a) Mean-Square-Displacement

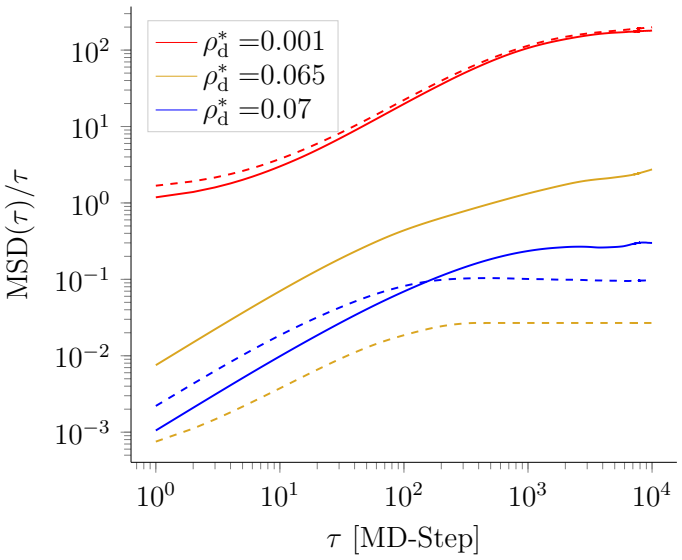

(b) Diffusion Coefficient

Figure 26: *Mean-Square-Displacement (a) and diffusion coefficient (b) for a dipole to active particle size ratio of 1:7.*

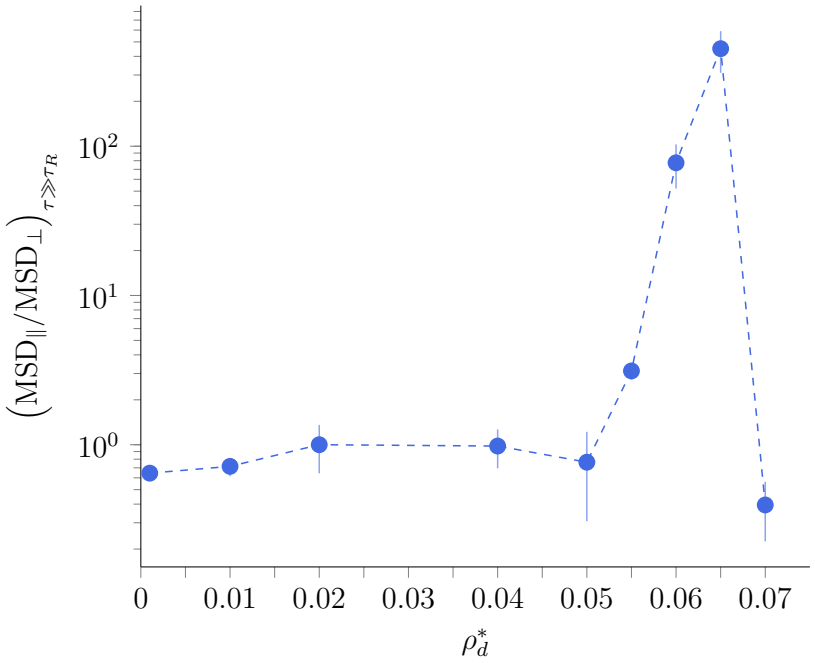

Figure 27: *Ratio of parallel to perpendicular diffusion, with respect to the applied magnetic field, at times much bigger than the relaxation time τ_r for a magnetic to active particle size ratio of 1:7. The peak efficiency occurs at ρ_d^* =0.065.*

Note that in figures 26 and 22, showing the mean square displacement, we experience a crossover between perpendicular and parallel components at the transition to the relaxed regime. The origin of this occurrence is not yet clear, and further investigation is needed but would go beyond the intentions of this thesis.

3.3 Size ratio 1:10

In figure 29a, additionally to the mean square displacement, two short black lines are plotted, showing the slope of the curve. This is done for the lowest density ρ_d=0.001 and resembles the trend of a free active particle as depicted in figure 8 by Bechinger et al., 2016.[3] This behaviour, though not explicitly marked, is the same for the 1:5 and 1:7 size ratios, which indicates that the active particle experiences an almost unbiased transport for the lowest density in all directions. The deviation from this behaviour for higher densities, especially along the x and y axis, shows again the influence of the magnetic particles on the swimmer.

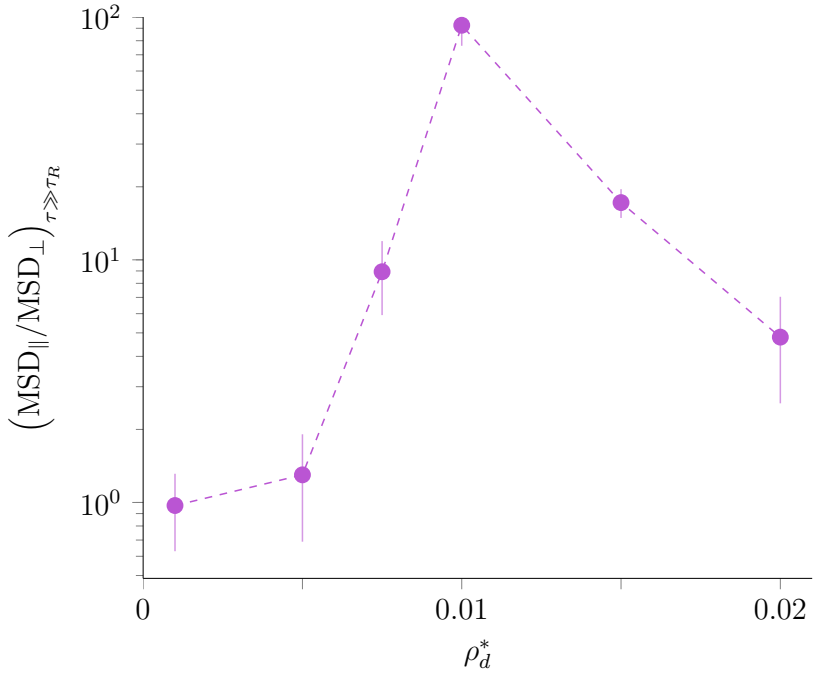

Figure 28: *Ratio of parallel to perpendicular diffusion, with respect to the applied magnetic field, at times much bigger than the relaxation time τ_r for a magnetic to active particle size ratio of 1:10. The peak efficiency occurs at ρ_d^* =0.01.*

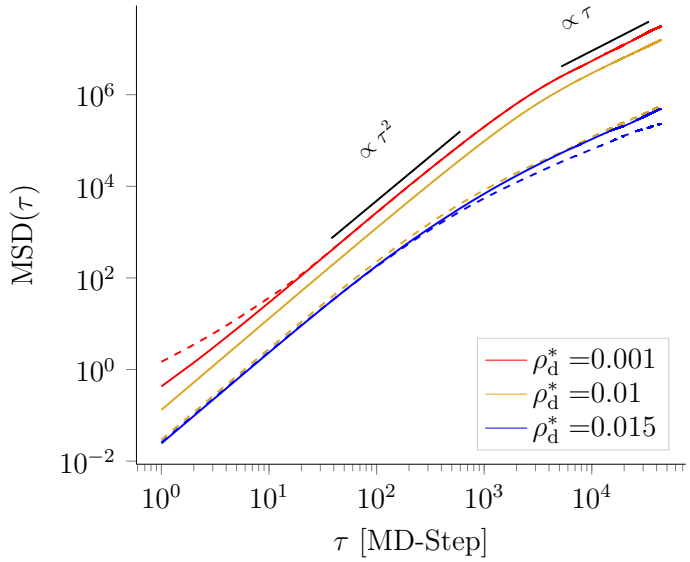

(a) Mean-Square-Displacement

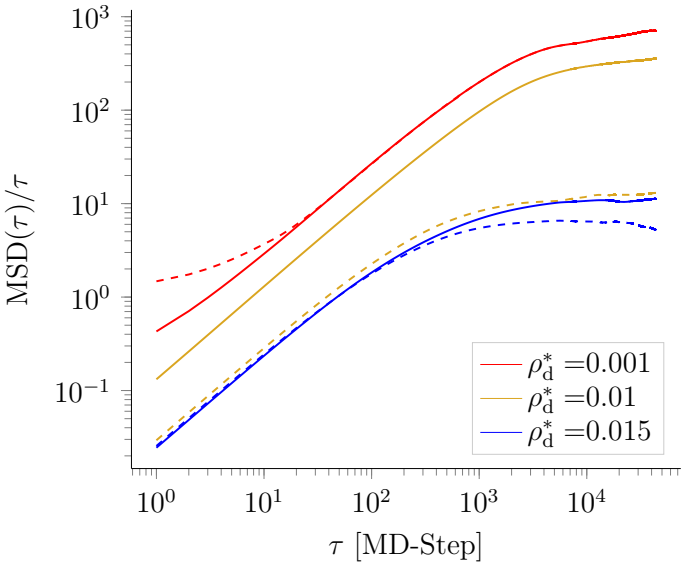

(b) Diffusion Coefficient

Figure 29: *Mean-Square-Displacement (a) and diffusion coefficient (b) for a dipole to active particle size ratio of 1:10. The black lines in (a) indicate the growing behaviour in the ballistic and diffusive regime of the curve.*

3.4 Comparison between different size ratios

Figure 30 combines the results for the ratios of parallel and perpendicular diffusion for all particle size ratios. The peak of the transport efficiency shifts to lower densities for bigger active particles, as suggested above. This means further, that we can find for each active particle size an optimal environmental density to maximize the transport efficiency in a desired direction, realized by the orientation of the applied magnetic field.

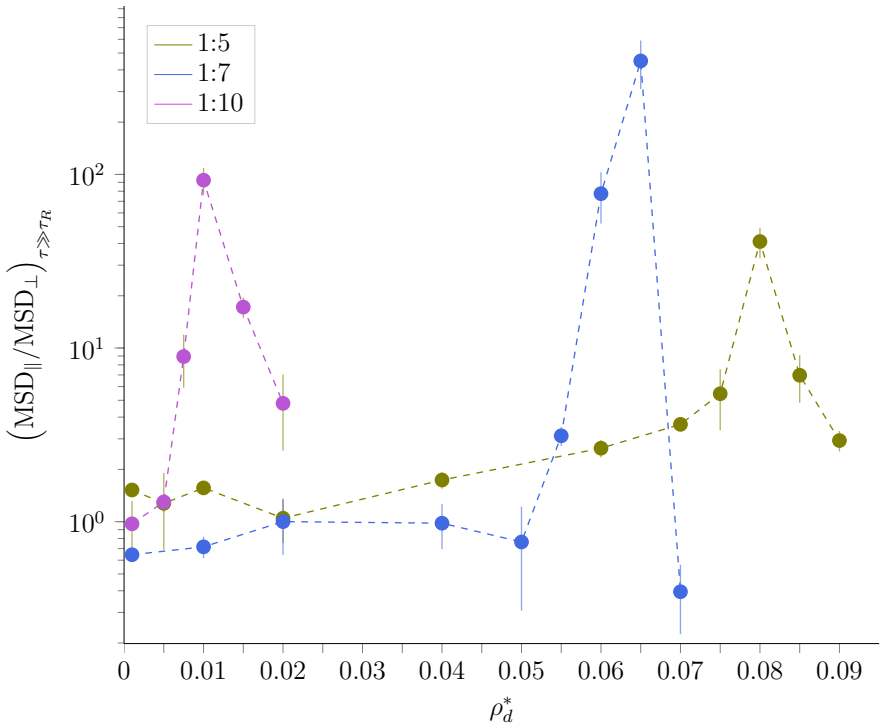

Figure 30: *Ratio of parallel to perpendicular diffusion, with respect to the applied magnetic field, at times much bigger than the relaxation time τ_r for magnetic to active particle size ratios of 1:5, 1:7 and 1:10. The peak efficiencies occur at ρ_d^* =0.1, 0.065 and 0.8, respectively.*

Those densities can be related to the features of the systems of magnetic particles. The incircle radii distributions shown in figure 31, correspond to the densities where the transport efficiency experiences a peak, with respect to particle size ratio. *It is seen, that the mean μ of the distribution, approximately coincides with the radius of the active particle, hence, the swimmer gets trapped in the perpendicular field direction if the tunnels are*

roughly equal to its own size. This result is crucial, as it gives us the ability to make a definite choice for the ferrofluid density depending on the size of the active particle, giving us greater control over the systems motion.

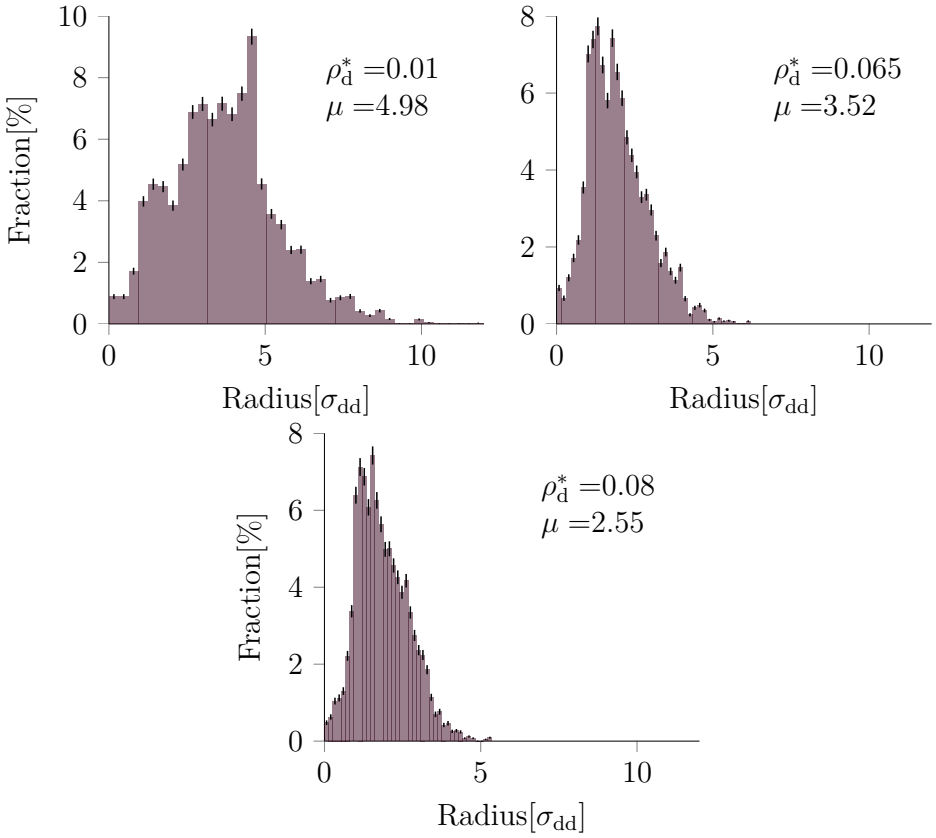

Figure 31: *Distribution of radii of the inscribed circles with mean μ, resulting from triangulating dipoles that are in the same x-y plane for densities at the peak transport efficiencies.*

4 Conclusion and outlook

Active matter research experienced a rapid growth over the past years, due to its significance in many fields such as biology, biomedicine, nanoscience and nanotechnology. The investigation of these systems, weather they are biological organisms or artificially created swimming colloids or nanomotors, brought up various models to theoretically study active matter by utilizing computer simulations.

Run-and-tumble dynamics were intensively used for the examination of bacterial motion as well as free[7] and constrainted partciles[23]. Langevin dynamics have been primarily employed to have a look at active Brownian particles and their diffusive behaviour, commonly using the SET- and RH-model[37] which differ in form of the velocity dependet friction coefficient in the Langevin equation. This diffusive behaviour is highly influenced by the environment the active particle finds itself in and might be used to affect its motion. Therefore, the active particle has to be set in an environment that can be controlled.

One example for this are fluids with magnetic particles, or simply ferrofluids. These consist of ferromagnetic particles and have been intensively studied over the past years, showing highly applicable properties. It is by now commonly known, that ferromagnetic particles tend to self-assemble if exposed to external magnetic or electric fields[17]. The most common formed shapes associated with this process are chains, but it has also been shown that in the absence of external fields, especially for high density fluids, the formation of rings, X-, Y- and Z-structures, up to complicated network structures is possible[20].

Combining these two phenomena, by using extensive molecular dynamic simulations, we introduce a theoretical approach to control the motion of a generic non magnetic active particle. The active particle is placed in a bath of ferromagnetic particles exposed to a magnetic field which causes chain formation along the field direction. The formed effective tunnels allow the

active particle to preferably move into the direction parallel to the applied external field and the efficiency of this motion for different sized swimmers, depends then on the density of the ferromagnetic particles. Analysis of this system reveals, that the maximum efficiency for the transport along the field direction appears at densities where the interaction distance is close to the active particles diameter. This novel result allows us to control non magnetic active matter with externally applied fields in magnetoresponsive environments.

Future studies could even further focus on this system, looking at velocity dependence of the active particle, magnetic coupling strength and hydrodynamic interactions. This might open up even more possibilities to take control of this system, increasing the transport efficiency.

Furthermore, there are some aspects that have to be mentioned regarding the investigated system. We were exploring an active particle with constant velocity. While in computer simulations this feature is easily implemented, it is not the case for experimental set-ups. It would be therefore interesting not to look at constant velocity, but constant force particles. This change could increase the studied effect of directional swimming, as a particle with constant velocity is more likely to break through a chain than just be directed by it.

A simplification in our model is the assumption of equally sized ferromagnetic particles. There, further investigation into polydisperse systems and their influence on the transport efficiency of active matter could add to the understanding of the effect.

The choice for the medium in which the ferromagnetic particles are suspended to create a ferrofluid is also of crucial physical importance. A standard choice for a solvent is kerosene, but organic active swimmers will not be able to swim in this medium and it is restricted to use with artificial particles only. Water based ferromagnetic fluids exist, but they are electrostatically stabilised. This means that the interactions between the active

particle and the charges have to be considered additionally.

The production of artificial active matter is another non trivial task, forcing scientists to invent new ways of synthesising these microscale particles. One idea to create controllable active motors, brought to life by Prof. Annette Schmidt from the university of Cologne[15], is to create cube shaped magnetic dipoles that provide the sensitivity to magnetic fields, and to attach spherical active particles to said cube which then provide the propulsion. A snapshot from a computer model for such a unit is seen in figure 32 .This project is now investigated in collaboration with Prof. Schmidt, experimentally and theoretically.

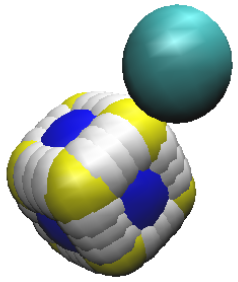

Figure 32: *Computer model of an active motor with cube shaped dipolar body and attached active swimmer (light blue)*

Appendices

A Appendix

For the computation of $C(t)$ in equation (35) and $w(t+\Delta t) - w(t)$ in equation (34), we use the property (32) of the wiener processes to show

$$\left\langle (w(t+\Delta t) - w(t))^2 \right\rangle = \left\langle w^2(t+\Delta t) + w^2(t) - 2w(t+\Delta t)w(t) \right\rangle = \Delta t.$$

The random variable $w(t+\Delta t) - w(t)$ can be generated at any timestep by using a gaussian distributed random number ξ with zero mean and unitary variance, as follows,

$$w(t+\Delta t) - w(t) = \sqrt{\Delta t}\xi. \tag{48}$$

For $C(t)$, we use again (32) to show:

$$\left\langle (w(t+\Delta t) - w(t)) \int_t^{t+\Delta t} ds'(w(s') - w(t)) \right\rangle = \frac{\Delta t^2}{2}, \tag{49}$$

$$\left\langle \int_t^{t+\Delta t} ds(w(s) - w(t)) \int_t^{t+\Delta t} ds'(w(s') - w(t)) \right\rangle = \frac{\Delta t^3}{3}. \tag{50}$$

Equation (50) can be fulfilled when

$$\int_t^{t+\Delta t} ds(w(s) - w(t)) = \Delta t^{3/2}\eta, \tag{51}$$

with η beeing a random number. A problem arises if the above equation and (48) is put into (50), as it is found that $\langle \xi\eta \rangle = 1/2$, meaning that the two random numbers are correlated. To avoid this, η is split into two uncorrelated random numbers ,

$$\eta = a\xi + b\theta,$$

where $\langle \xi\theta \rangle = 0$ and $\langle \theta^2 \rangle = 1$. a and b can be determined if one imposes $\langle \xi\eta \rangle = 1/2$ and $\langle \eta^2 \rangle = 1/3$, which leads to $a = 1/3$ and $b = 1/(2\sqrt{3})$. This

finally leads to:

$$\int_t^{t+\Delta t}(w(s)-w(t))ds = \Delta t^{3/2}\left(\frac{\xi}{\sqrt{3}}+\frac{\theta}{2\sqrt{3}}\right), \tag{52}$$

which is the result as shown in (37).

References

[1] L Abdelmohsen et al. “Micro-and nano-motors for biomedical applications”. In: *Journal of Materials Chemistry B* 2.17 (2014), pp. 2395–2408.

[2] A Arnold et al. “Espresso 3.1: Molecular dynamics software for coarse-grained models”. In: *Meshfree methods for partial differential equations VI*. Springer, 2013, pp. 1–23.

[3] C Bechinger et al. “Active particles in complex and crowded environments”. In: *Reviews of Modern Physics* 88.4 (2016), p. 045006.

[4] CJ Brokaw. “Chemotaxis of bracken spermatozoids: the role of bimalate ions”. In: *Journal of Experimental Biology* 35.1 (1958), pp. 192–196.

[5] PJ Camp, JC Shelley, and GN Patey. “Isotropic fluid phases of dipolar hard spheres”. In: *Physical review letters* 84.1 (2000), p. 115.

[6] JJ Cerda et al. “P 3 M algorithm for dipolar interactions”. In: *The Journal of chemical physics* 129.23 (2008), p. 234104.

[7] A Costanzo. “Dynamics of Self-Propelled Particles: Diffusion, Motility-Sorting, and Rectification”. PhD thesis. Universität zu Köln, 2015.

[8] B Delaunay. “Sur la sphere vide”. In: *Izv. Akad. Nauk SSSR, Otdelenie Matematicheskii i Estestvennyka Nauk* 7.793-800 (1934), pp. 1–2.

[9] R Di Leonardo et al. “Swimming with an image”. In: *Physical review letters* 106.3 (2011), p. 038101.

[10] PP Ewald. “Die Berechnung optischer und elektrostatischer Gitterpotentiale”. In: *Annalen der Physik* 369.3 (1921), pp. 253–287.

[11] P Gonnet. “A simple algorithm to accelerate the computation of non-bonded interactions in cell-based molecular dynamics simulations”. In: *Journal of Computational Chemistry* 28.2 (2007), pp. 570–573.

[12] MM Hanczyc et al. “Fatty acid chemistry at the oil- water interface: Self-propelled oil droplets”. In: *Journal of the American Chemical Society* 129.30 (2007), pp. 9386–9391.

[13] H Helmholtz. *On the sensations of tone*. Courier Corporation, 2013.

[14] JR Howse et al. "Self-motile colloidal particles: from directed propulsion to random walk". In: *Physical review letters* 99.4 (2007), p. 048102.

[15] *http://www.nanomat.uni-koeln.de/schmidt.html*.

[16] PH Hünenberger. "Optimal charge-shaping functions for the particle–particleparticle–mesh (P3M) method for computing electrostatic interactions in molecular simulations". In: *The Journal of Chemical Physics* 113.23 (2000), pp. 10464–10476.

[17] A Hynninen and M Dijkstra. "Phase behavior of dipolar hard and soft spheres". In: *Physical review E* 72.5 (2005), p. 051402.

[18] HS Jennings. "On the significance of the spiral swimming of organisms". In: *The American Naturalist* 35.413 (1901), pp. 369–378.

[19] J Joanny, F Jülicher, and J Prost. "Motion of an adhesive gel in a swelling gradient: a mechanism for cell locomotion". In: *Physical review letters* 90.16 (2003), p. 168102.

[20] SS Kantorovich et al. "Temperature-induced structural transitions in self-assembling magnetic nanocolloids". In: *Physical Chemistry Chemical Physics* 17.25 (2015), pp. 16601–16608.

[21] I Karatzas and S Shreve. *Brownian motion and stochastic calculus*. Vol. 113. Springer Science & Business Media, 2012.

[22] PM Kareiva and N Shigesada. "Analyzing insect movement as a correlated random walk". In: *Oecologia* 56.2 (1983), pp. 234–238.

[23] M Khatami et al. "Active Brownian particles and run-and-tumble particles separate inside a maze". In: *Scientific reports* 6 (2016), p. 37670.

[24] N Komin, U Erdmann, and L Schimansky-Geier. "Random walk theory applied to daphnia motion". In: *Fluctuation and Noise Letters* 4.01 (2004), pp. L151–L159.

[25] F Kümmel et al. "Circular motion of asymmetric self-propelling particles". In: *Physical review letters* 110.19 (2013), p. 198302.

[26] P Langevin. "Sur la théorie du mouvement brownien". In: *CR Acad. Sci. Paris* 146.530-533 (1908), p. 530.

[27] E Lauga et al. “Swimming in circles: motion of bacteria near solid boundaries”. In: *Biophysical journal* 90.2 (2006), pp. 400–412.

[28] Y Magariyama et al. “Difference in bacterial motion between forward and backward swimming caused by the wall effect”. In: *Biophysical journal* 88.5 (2005), pp. 3648–3658.

[29] TJ Mitchison and LP Cramer. “Actin-based cell motility and cell locomotion”. In: *Cell* 84.3 (1996), pp. 371–379.

[30] Catalytic Nanomotors. “Autonomous Movement of Striped Nanorods Paxton”. In: *Walter F* (), pp. 13424–13431.

[31] S Odenbach. “Ferrofluidsmagnetically controlled suspensions”. In: *Colloids and Surfaces A: Physicochemical and Engineering Aspects* 217.1-3 (2003), pp. 171–178.

[32] RW Pastor, BR Brooks, and A Szabo. “An analysis of the accuracy of Langevin and molecular dynamics algorithms”. In: *Molecular Physics* 65.6 (1988), pp. 1409–1419.

[33] WF Paxton, Kevin C Kistler, and Christine C Olmeda. “Catalytic nanomotors: autonomous movement of striped nanorods”. In: *Journal of the American Chemical Society* 126.41 (2004), pp. 13424–13431.

[34] FS Peruani et al. “Collective motion and nonequilibrium cluster formation in colonies of gliding bacteria”. In: *Physical review letters* 108.9 (2012), p. 098102.

[35] Lord Rayleigh. *The Theory of Sound. Mac Millan.* 1945.

[36] P Reimann. “Brownian motors: noisy transport far from equilibrium”. In: *Physics reports* 361.2 (2002), pp. 57–265.

[37] P Romanczuk et al. “Active brownian particles”. In: *The European Physical Journal Special Topics* 202.1 (2012), pp. 1–162.

[38] F Schweitzer, W Ebeling, and B Tilch. “Complex motion of Brownian particles with energy depots”. In: *Physical Review Letters* 80.23 (1998), p. 5044.

[39] S Sundararajan et al. “Catalytic motors for transport of colloidal cargo”. In: *Nano letters* 8.5 (2008), pp. 1271–1276.

[40] J Tailleur and ME Cates. “Sedimentation, trapping, and rectification of dilute bacteria”. In: *EPL (Europhysics Letters)* 86.6 (2009), p. 60002.

[41] I Theurkauff et al. “Dynamic clustering in active colloidal suspensions with chemical signaling”. In: *Physical review letters* 108.26 (2012), p. 268303.

[42] GE Uhlenbeck and LS Ornstein. “On the theory of the Brownian motion”. In: *Physical review* 36.5 (1930), p. 823.

[43] E Vanden-Eijnden and G Ciccotti. “Second-order integrators for Langevin equations with holonomic constraints”. In: *Chemical physics letters* 429.1-3 (2006), pp. 310–316.

[44] J Vicario et al. “Catalytic molecular motors: fuelling autonomous movement by a surface bound synthetic manganese catalase”. In: *Chemical Communications* 31 (2005), pp. 3936–3938.

[45] A Walther and AH Müller. “Janus particles”. In: *Soft Matter* 4.4 (2008), pp. 663–668.

[46] S Wang and N Wu. “Selecting the swimming mechanisms of colloidal particles: bubble propulsion versus self-diffusiophoresis”. In: *Langmuir* 30.12 (2014), pp. 3477–3486.

[47] Z Wang, C Holm, and HW Müller. “Molecular dynamics study on the equilibrium magnetization properties and structure of ferrofluids”. In: *Physical Review E* 66.2 (2002), p. 021405.

[48] HH Wensink et al. “Meso-scale turbulence in living fluids”. In: *Proceedings of the National Academy of Sciences* 109.36 (2012), pp. 14308–14313.

[49] J Yan et al. “Reconfiguring active particles by electrostatic imbalance”. In: *Nature materials* 15.10 (2016), pp. 1095–1099.

[50] M Yang and M Ripoll. “Simulations of thermophoretic nanoswimmers”. In: *Physical Review E* 84.6 (2011), p. 061401.

[51] Y Yang, V Marceau, and G Gompper. “Swarm behavior of self-propelled rods and swimming flagella”. In: *Physical Review E* 82.3 (2010), p. 031904.

[52] H Zhang et al. "Collective motion and density fluctuations in bacterial colonies". In: *Proceedings of the National Academy of Sciences* 107.31 (2010), pp. 13626–13630.

[53] J Zhang, J Yan, and S Granick. "Directed Self-Assembly Pathways of Active Colloidal Clusters". In: *Angewandte Chemie International Edition* 55.17 (2016), pp. 5166–5169.